

3D Motion Manipulation for Micro- and Nanomachines: Progress and Future Directions

Hai Huang, Shihao Yang, Yulong Ying,* Xiangzhong Chen,* Josep Puigmartí-Luis,* Li Zhang,* and Salvador Pané*

In the past decade, micro- and nanomachines (MNMs) have made outstanding achievements in the fields of targeted drug delivery, tumor therapy, microsurgery, biological detection, and environmental monitoring and remediation. Researchers have made significant efforts to accelerate the rapid development of MNMs capable of moving through fluids by means of different energy sources (chemical reactions, ultrasound, light, electricity, magnetism, heat, or their combinations). However, the motion of MNMs is primarily investigated in confined two-dimensional (2D) horizontal setups. Furthermore, three-dimensional (3D) motion control remains challenging, especially for vertical movement and control, significantly limiting its potential applications in cargo transportation, environmental remediation, and biotherapy. Hence, an urgent need is to develop MNMs that can overcome self-gravity and controllably move in 3D spaces. This review delves into the latest progress made in MNMs with 3D motion capabilities under different manipulation approaches, discusses the underlying motion mechanisms, explores potential design concepts inspired by nature for controllable 3D motion in MNMs, and presents the available 3D observation and tracking systems.

1. Introduction

Micro- and nanomachines (MNMs) were proposed by the Nobel laureate Richard Feynman in 1959, who suggested that tiny-scale objects could be implanted in the body to address medical conditions in a minimally invasive approach.^[1] In nature, creatures, including bacteria, insects, fishes, and birds, can perceive changes in the environment and execute a series of complex motion behaviors (including individuals and swarms), such as navigating through narrow and curved passages, evading obstacles, hunting, and even launching attacks against enemies.^[2] Inspired by the complex motion behaviors of motile creatures, scientists from different fields have developed artificial machines at multiple scales, i.e., centimeter/millimeter,^[3] micrometer/nanometer,^[4] and molecular levels.^[5] In the last two decades, significant attention has been devoted to exploring


H. Huang, Y. Ying
School of Materials Science and Engineering
Zhejiang Sci-Tech University
Hangzhou 310018, China
E-mail: yingyulong@zstu.edu.cn

S. Yang, L. Zhang
Department of Mechanical and Automation Engineering
the Chinese University of Hong Kong
Shatin, N.T., Hong Kong 999077, China
E-mail: lizhang@mrc-cuhk.com

X. Chen
Institute of Optoelectronics
State Key Laboratory of Photovoltaic Science and Technology
Shanghai Frontiers Science Research Base of Intelligent Optoelectronics and Perception
Fudan University
Shanghai 200433, China
E-mail: xzchen@fudan.edu.cn

J. Puigmartí-Luis
Departament de Ciència dels Materials i Química Física
Institut de Química Teòrica i Computacional
University of Barcelona (UB)
Barcelona 08028, Spain
E-mail: josep.puigmarti@ub.edu

J. Puigmartí-Luis
Institució Catalana de Recerca i Estudis Avançats (ICREA)
Pg. Lluís Companys 23, Barcelona 08010, Spain
S. Pané
Multi-Scale Robotics Lab
Institute of Robotics and Intelligent Systems
ETH Zürich
Tannenstrasse 3, Zürich CH-8092, Switzerland
E-mail: vidalp@ethz.ch

 The ORCID identification number(s) for the author(s) of this article can be found under <https://doi.org/10.1002/adma.202305925>

© 2023 The Authors. Advanced Materials published by Wiley-VCH GmbH. This is an open access article under the terms of the Creative Commons Attribution-NonCommercial License, which permits use, distribution and reproduction in any medium, provided the original work is properly cited and is not used for commercial purposes.

DOI: 10.1002/adma.202305925

the fundamentals governing micro- and nanoscale objects' motion within the field of MNMs.^[6] Artificial MNMs are micro- and nanodevices that can convert environmental energy (i.e., chemical, acoustic, photonic, electric, magnetic, thermal) into mechanical motion.^[7] Unlike traditional colloidal particles that exhibit only Brownian motion in thermal equilibrium, MNMs are distinguished for their self-motion abilities. As micro- and nanotechnology and materials science continue to advance, researchers can now manufacture MNMs with various structures and properties using organic, inorganic, and biological materials.^[8] MNMs have shown outstanding potential in various fields, such as targeted drug delivery, tumor treatment, micro- and nanosurgery, biological detection, and environmental monitoring and remediation.^[9]

However, the precise motion control of the MNMs remains one of the most challenging issues in this field. In recent years, great efforts have been dedicated toward triggering and controlling the motion of MNMs.^[6d,10] In the absence of external stimuli, MNMs exhibit random and irregular Brownian motion in fluids. Conversely, when exposed to energy sources (chemical, magnetic, sound, light, electric fields, or their combinations), MNMs can perform specific motion trajectories, such as straight lines, circles, spirals, and other complex motion behaviors. Motion-braking, acceleration-deceleration, and diffusion-gathering could also be identified among others.^[11] Unfortunately, most MNMs designed with traditional materials are usually easy to settle at the bottom of the solution because of their weight and insufficient driving force, which limits their widespread application. While most efforts have been focused on regulating the two-dimensional (2D) motion of MNMs, achieving three-dimensional (3D) motion, especially in the vertical direction, remains a relatively unexplored area. Achieving control over the motion in the Z-axis direction is a challenging endeavor in the field of MNMs, and significant progress has yet to be made. However, its significance spans both fundamental research and subsequent applications. The regulation of the MNMs' 3D motion is key, for example, for environmental remediation applications in complex media or confined spaces. In this context, control over 3D motion will not only allow for precise control over the MNMs against gravity but also facilitate microregion stirring, improving mass transfer effects in solutions, enhancing the capture and adsorption of target molecules, and ultimately boosting chemical reactions. In summary, 3D motion can significantly improve the efficiency of catalytic, adsorption, and separation processes.^[9b] Achieving controlled 3D motion is also key in biomedicine, as it enables MNMs to load and release drugs in difficult-to-reach targeted biological tissues. MNMs with 3D motion capabilities can navigate through intricate biological environments, narrow blood vessels and ultimately penetrate barriers to target specific lesion sites.^[12] Currently, bubble recoil propulsion is the simplest way for MNMs to move in the Z-axis direction, but it has limitations due to the need for toxic chemicals (such as hydrogen peroxide and surfactants) and the lack of trajectory and speed control.^[6b] Besides, the excessively generated bubbles can cause some undesirable effects. For example, bubbles may disrupt the dynamical evolution of the gas-liquid interface in confined spaces, leading to suppressed diffusion and bubble accumulation at the top of the containers, i.e., the bubble foam layer. This layer can scatter light and draw active species to the top of the containers, ulti-

mately reducing the reaction contact area and leading to poor adsorption and degradation performance.^[13] Another critical limitation of bubble-propelled MNMs is their limited biocompatibility characteristics for medical applications. By contrast, external-field-propelled MNMs represent a more attractive method for 3D motion control compared to bubble-propelled method due to their advantages of fast actuation, strong variable force, wireless and precise control, and high biocompatibility features. Advancements in magnetic, acoustic, optical, and electric stimuli have been made,^[14] but there is still a need for further progress in this area.

This review aims to provide an up-to-date overview of recent developments in 3D motion control for MNMs in recent years, especially in the vertical direction (**Figure 1**). We discuss several strategies for controlling the 3D motion of MNMs using external energy inputs, such as light, magnetic fields, ultrasound, electric fields, or their combinations. Then, we briefly introduce the Z-axis motion behavior of centimeter/millimeter-scale motors to provide guidance on potential theoretical and practical methods for designing MNMs with 3D controllable motion behavior. Furthermore, we highlight recent developments and advances in current observation and tracking techniques for 3D motion. Finally, we discuss future challenges and opportunities in this field. We also suggest new design concepts inspired by bacteria to swim against gravity, such as bionic flagella, which uses pushing forces, gas vesicles with buoyancy regulation, and combinations of these approaches. We believe this review can stimulate research interest and accelerate the development of 3D motile small-scale devices.

2. Externally Controlled Z-Axis Motion of MNMs

Motion control in the Z-axis direction is a critical and challenging problem with significant implications for both fundamental research and practical applications. In aqueous environments, MNMs are subject to various forces that require a careful attention in order to compensate gravity and achieve control over the vertical motion (**Figure 2**). Control over the self-gravity of a body can be achieved by regulating the driving forces in the Z-axis, which include buoyancy and external driving forces. A commonly investigated method for regulating the vertical driving force is, for example, by mimicking the motion mechanism of bacterial flagella. Vertical-driven force regulation is the most widely studied method among the various strategies for achieving the Z-axis motion control in MNMs. However, in order to achieve propulsion in any direction, a horizontal force must also be present alongside the vertical force. An externally driven force with variable direction would be the most effective solution. Currently, bubble propulsion based on the catalytic decomposition of H_2O_2 is the most widely adopted approach due to its strong driving force and ability to achieve 3D motion.^[15] Yet, the excessive formation and release of bubbles, coupled with the unavoidable use of surfactants, result in inadequate directionality and speed control and unpredictable adverse effects. These issues pose obvious challenges for their use in the field of medicine. By contrast, external-field-propelled MNMs represent a more attractive method for 3D motion control than the bubble propulsion approach because of fast actuation, force tunability, wireless and precise control, and high biocompatibility features.

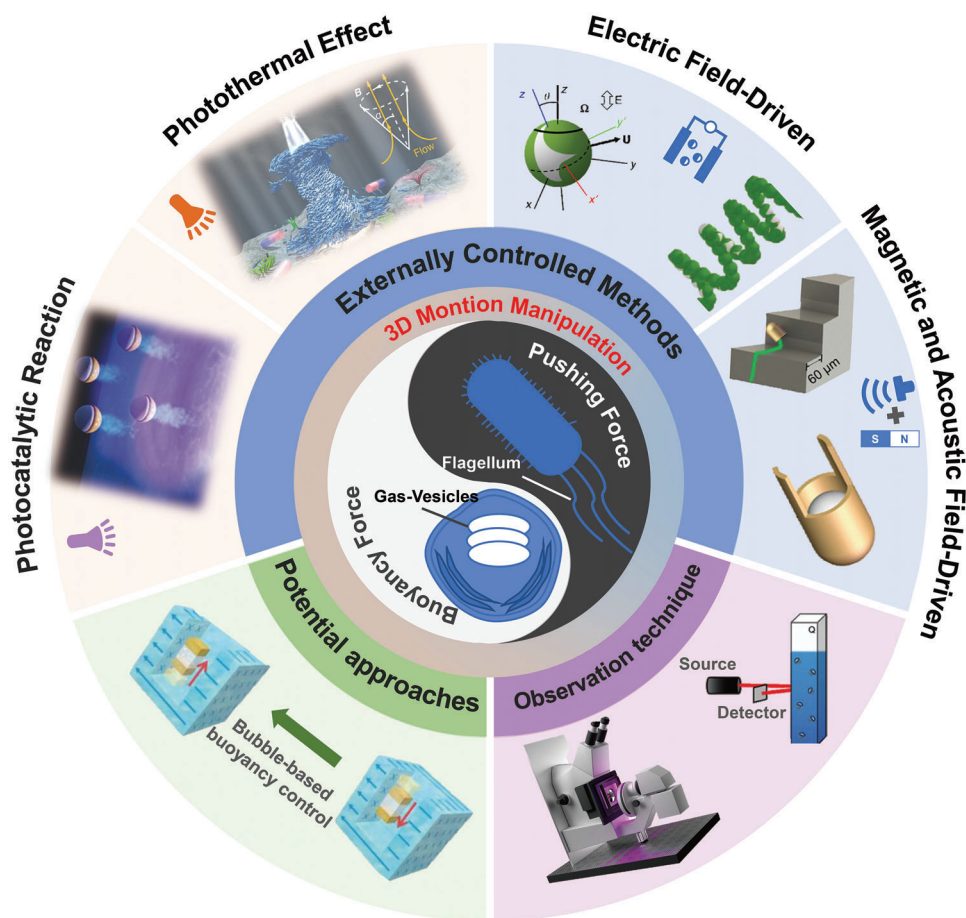


Figure 1. Current advances in MNMs for 3D motion.

Consequently, the focus of our review is on current advances in the 3D motion of MNMs by means of external power sources, such as light, acoustic, magnetic, and electric fields, or their combinations.

2.1. Light-Driven MNMs

Light actuation is appealing for powering and controlling MNMs because of its noncontact nature, simple equipment, easy system integration, and flexibility in adjusting parameters such as light beam size, intensity, wavelength, incident angle, and phase.^[16] Thanks to these features, fuel-free light-driven MNMs can be efficiently powered and controlled with a high degree of freedom in time and space.^[17] Currently, light-driven MNMs could be broadly classified into photophysically and photochemically driven swimmers based on the operating principles. Photothermally driven MNMs are one kind of photophysical MNMs that require the integration of photothermal materials into the structural design, typically including organic photothermal materials, carbon materials, and noble metals.^[18] Photochemically propelled MNMs utilize light to trigger photochemical reactions such as photochromic or photocatalytic effects to convert photonic energy into mechanical energy to generate motion by several mechanisms, including self-diffusiophoresis, self-

electrophoresis, and bubble propulsion.^[19] However, achieving motion in the Z-axis direction can be challenging.^[20] Conventional light-driven MNMs based on photochemical mechanisms, particularly those based on inorganic semiconductor materials, are typically limited to 2D planar motion at the bottom of the solution container due to their high density and limited driving force. By contrast, some MNMs based on the photothermal effect could achieve 3D motion behavior.^[21] Therefore, current developments on light-driven MNMs with 3D motion are described in two sections based on the intrinsic properties of the photoactive materials or the interaction between light and matter, i.e., the photothermal effect and photocatalysis.

2.1.1. Photothermal Effect

Photothermal effects have been widely observed in various materials through energy conversion from light to heat, producing hot fluid or hot air that could generate convection and lead to a 3D motion.^[22] In 2014, Cohen and Golestanian realized a theoretical breakthrough by conducting a simulation of a light-driven colloidal system.^[23] The Z-axis displacement could be realized by the thermal gradient produced by light radiation, where the colloidal particles spontaneously showed vertical self-organization and formed a long-term comet-like swarm. Rich

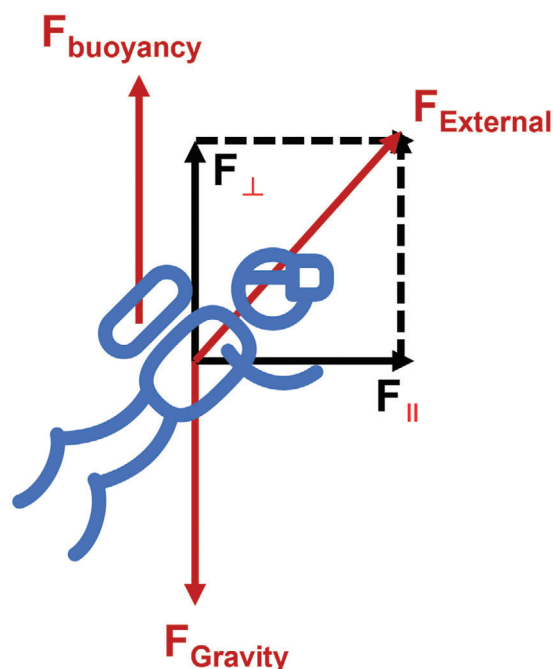


Figure 2. Force analysis of MNMs in an aqueous solution, considering self-gravity, buoyancy, and an externally driven force. The external force can be broken down into its vertical (F_{\perp}) and horizontal (F_{\parallel}) components.

dynamic swarm behaviors were shown by adjusting the light power density using a Brownian dynamics simulation. Near-infrared (NIR) light has been recognized as an ideal energy source for powering artificial MNMs. So far, the conventional strategies reported to drive MNMs by NIR light mainly rely on thermally responsive asymmetric structures (e.g., Janus and tubular MNMs), where the thermophoresis force occurs due to the existing asymmetric local temperature gradients.^[24] Generally, developing and producing asymmetric light-triggered MNMs typically involve time-consuming, low-yield, and challenging processes.^[25] Recently, Jiao and co-workers reported a size-controllable reduced graphene oxide (rGO) aerogel sphere micromotor easily by one-step electrospraying (Figure 3a).^[21a] The fast movement of the micromotor driven by NIR light is attributed to the low weight of the aerogel and the high photothermal conversion capacity of rGO. This system does not require an asymmetrical structure or composition for its propulsion. The precise tuning of the micromotor's properties could be achieved by carefully controlling the reduction degree and soaking time of the graphene oxide. The as-prepared rGO-based micromotors are able to absorb water gradually, increase their weight, and sink to the bottom of a solution. Interestingly, when irradiated with NIR light, the micromotors exhibit a rapid ascending motion similar to that of a submarine. This upward motion is driven by the energy conversion of light into heat, which raises the internal temperature of the porous microspheres and leads to the conversion of internal water into water vapor. The resulting bubbles generate a buoyancy force that overcomes the self-gravity of the micromotors and propels them upward. Conversely, when the NIR light was turned off, the micromotors would sink back to the bottom due to the vanish-

ment of the bubbles and the weight increase in water absorption (Figure 3b). The rGO-based micromotors are capable of repeating this cycle of ascending and descending without attenuation by the NIR light on/off switch. It means that these NIR-driven micromotors could be positioned at any depth in the aqueous solution through light regulation, which includes adjusting, for instance, the power density, irradiation direction, or beam spot size.

Zhang and co-workers proposed an innovative approach to combine magnetic fields and light to generate a 3D microswarm tornado (MST) from a 2D microswarm (Figure 3c).^[21b] The 3D MST goes through four distinct stages: rising, hovering, oscillation, and landing, making this approach effective in capturing model contaminants for water pollution remediation. To form 2D microgroups, $\text{Fe}_3\text{O}_4@SiO_2$ nanoparticles (NPs) must converge on the substrate aided by an optimal magnetic field. The use of NIR light enables the individual $\text{Fe}_3\text{O}_4@SiO_2$ particles to move into a more densely packed microswarm (Figure 3d), which then spirals upward above the substrate to gradually form the 3D MST due to the induced upward convection flow caused by the hybrid energy source. The resulting 3D MST is in a long-term dynamic hovering state, facilitating its potential application in regulating the common chemical reaction rate. The 3D MST was used to degrade methylene blue (MB) in a solution containing ascorbic acid. In line with Bernoulli's principle,^[26] the high circulation velocity at the distal area of the MST during its rotational motion enhanced the degradation of MB. However, the solution at the proximal area and the center of the tornado-like microswarm was almost steady, leading to a low degradation efficiency. To overcome this limitation, the applied magnetic field can be modulated to oscillate in the XZ- and YZ-planes, resulting in a faster degradation of the MB. While the 3D MST can trap the target object and perform the Z-axis mass transportation during the reconfigurable rising and landing stages, simultaneously manipulating the magnetic fields and the light is complicated and challenging.

Sun and co-workers synthesized microscale multiwavelength phototactic micromotors based on $\text{Fe}_3\text{O}_4@poly(\text{glycidyl methacrylate})/polystyrene$ ($\text{Fe}_3\text{O}_4@PGS$) core-shell particles with high photothermal conversion efficiency.^[21c] The micromotors exhibited phototactic behavior, in other words, they moved toward the light source due to a convective flow generated by a temperature gradient between the irradiated and nonirradiated areas. The hydrodynamic resistance in the Z-axis direction eased the movement of the micromotors toward the light spot (Figure 3e,f). The study demonstrated that these light-driven micromotors accelerated the degradation of rhodamine B through the Fenton reaction, which is induced by Fe_3O_4 NPs. Furthermore, these micromotors enhanced the enzymatic reaction ability in organic solutions. Ying and co-workers designed versatile multiwavelength light-responsive PCN-224-metal-organic-framework-based micromotors (MOFtors) comprising a metallated porphyrin tetra-kis(4-carboxyphenyl)porphyrin (TCPP). These micromotors were designed for water sterilization purposes.^[27] Besides serving as a key structural building block in manufacturing the PCN-224-MOF-based motors, TCPP acted as a photothermal sensitive component. Additionally, metal ions were doped to adjust the light absorption, the photothermal conversion, and the photochemical properties of the system, which ultimately serve to

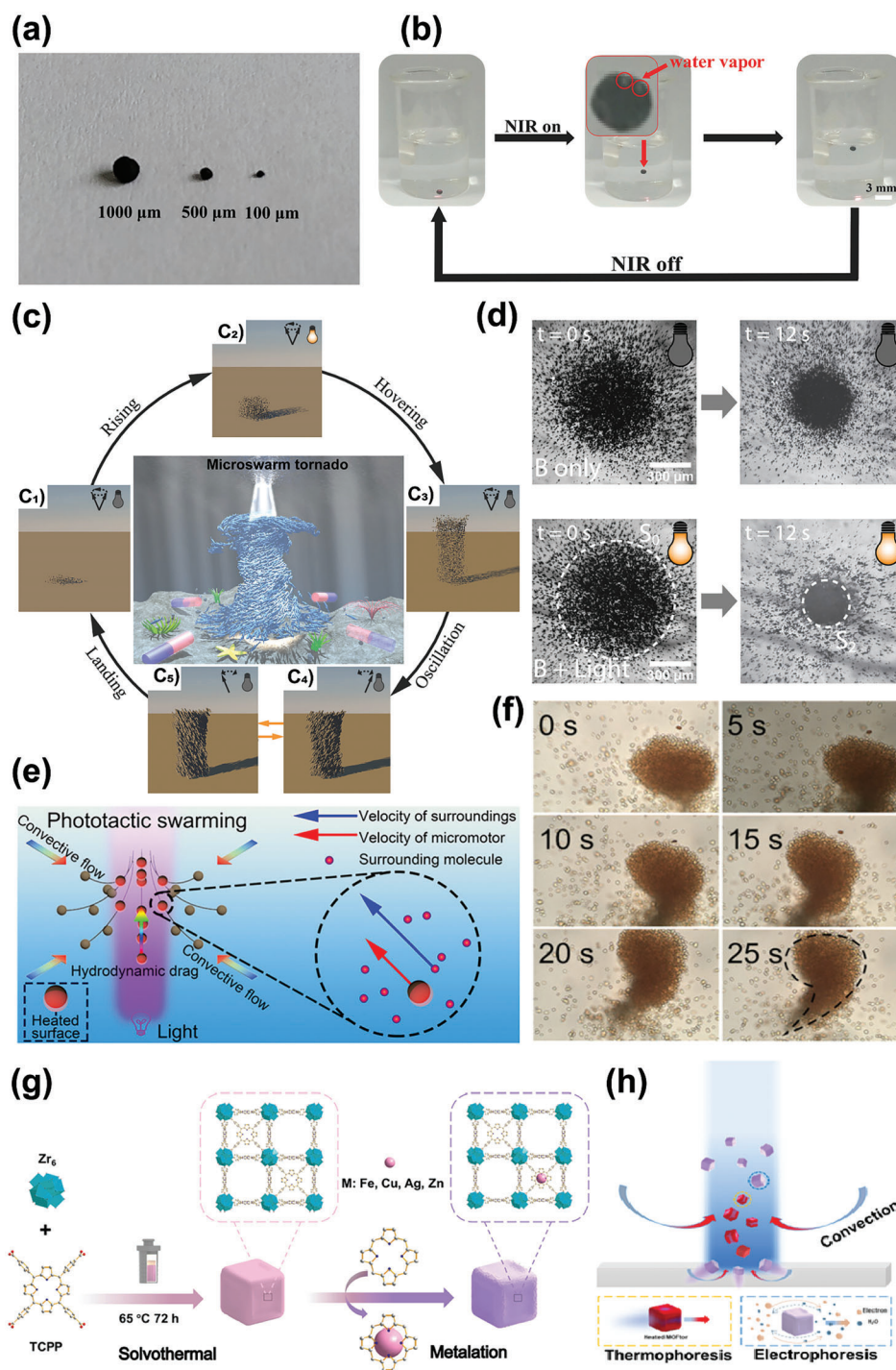


Figure 3. 3D motion of MNMs based on the photothermal effect. a) Optical image showing different sizes of rGO aerogel sphere prepared using the electro spraying method. b) Photographs of the micromotor floating and sinking in the water. When the micromotor is irradiated by NIR, the water vapor generated inside increases the buoyancy of the micromotor. Reproduced with permission.^[21a] Copyright 2020, American Chemical Society. c) Image illustrating the whole process of establishing a reconfigurable a microswarm tornado. c₁–c₅) Schematics show in detail the four processes, including rising, hovering, oscillation, and landing. d) Digital images of the microswarm when a magnetic field is applied only and when both magnetic field and light irradiation are applied simultaneously. The latter approach leads to a close-packed microswarm. Reproduced with permission.^[21b] Copyright 2020, American Chemical Society. e) Schematic diagram of Fe₃O₄@PGS micromotor driven by photothermal induced hydrodynamic resistance. In the experiment, the intensity of the light is 127 mW cm⁻², and the length of the arrow indicates the speed. f) Time-lapse images of clusters formed by Fe₃O₄@PGS micromotors driven by UV light irradiation of 22 mW cm⁻². Reproduced with permission.^[21c] Copyright 2020, American Chemical Society. g) Schematic representation of the preparation of PCN-224(H) and metal ions modified PCN-224(M). h) Schematic diagram illustrating the motion of PCN-224(H) and PCN-224(M)-based MOFtors during blue light irradiation. Reproduced with permission.^[27] Copyright 2023, Wiley-VCH GmbH.

modulate the motion behavior and water sterilization performance of the MOFtors.

2.1.2. Photocatalysis

Light-powered MNMs have generated considerable interest, with photocatalytic Janus MNMs being among the most intensively investigated. Janus MNMs consist of photocatalytic semiconductor particles (e.g., TiO_2 , ZnO , Fe_2O_3) asymmetrically coated with metal layers (e.g., Pt, Au).^[28] During photocatalysis, a gradient of reactants or products is generated around the particles owing to either the asymmetric structure of MNMs or the exposure to light gradients. The photogenerated chemical species can be soluble ionic or nonionic, resulting in electrophoretic or diffusiophoretic motion, respectively. Additionally, photogeneration of gas can also take place and result in relatively large bubbles, which can also contribute to the 3D motion of MNMs.^[4a,29]

Dong and co-workers developed micromotors comprising graphite-like carbon nitride decorated with cocatalytic Pt nanoparticles ($\text{Pt/g-C}_3\text{N}_4$).^[30] $\text{Pt/g-C}_3\text{N}_4$ is a highly efficient photocatalyst.^[31] When exposed to light, the ionic products generated by photocatalytic reactions display varying diffusion rates on two sides, creating an electric field around the micromotor. As a result, the micromotors exhibit positive phototaxis, which means they move toward the light source due to the negative charge on the $\text{Pt/g-C}_3\text{N}_4$ surface (Figure 4a). When a highly concentrated electrolyte (NaCl) is introduced, the micromotor does not move under light irradiation, indicating that the self-diffusiophoresis is the governing motion mechanism. The researchers also investigated the collective swarm behavior of the $\text{Pt/g-C}_3\text{N}_4$ micromotors. Initially, the micromotors settle at the bottom of the solution due to gravity. When vertically illuminated with light, a swarm of micromotors moved toward the center of the light source, in contrast to a single micromotor, which did not move significantly. With increased light energy, the driving force of the micromotors becomes large enough to overcome gravity and move rapidly in the vertical direction, resulting in a highly turbulent solution system (Figure 4b). Interestingly, surface modification of $\text{Pt-g-C}_3\text{N}_4$ with an amine end-functionalized thiol resulted in a positively charged $\text{NH}_2\text{-Pt/g-C}_3\text{N}_4$ in solution, which showed a negative phototaxis behavior under light irradiation. Previous research has shown that for light-driven MNMs to move against gravity, the incident light needs to be properly aligned with the direction of the gravitational force to provide enough thrust to overcome gravity.^[32] This requires specific particle design and defined lighting to achieve motion in the Z-axis.^[16a] In this vein, a “geometrical shadowing” effect concept was reported by Fischer and co-workers,^[33] i.e., a portion of the photocatalyst on the micromotor was active only when it was directly exposed to light irradiation.^[34] The light-driven Janus micromotors based on spherical SiO_2 particles were fabricated by coating a hemisphere with a layer of anatase TiO_2 (Figure 4c). The motion of two kinds of photochemically active micromotors with radii of $R = 0.5$ and $1.0 \mu\text{m}$ (the radius of the SiO_2 sphere) was studied in a 2% H_2O_2 solution. When the bottom of the solution was illuminated by UV light, the “catalytic cap” of the micromotor produced a chemical concentration gradient via photocatalysis to promote its movement. A theoretical model

supported by experimental evidence revealed that three factors affected the characteristic speed of the micromotor, i.e., light-induced activity, bottom heaviness, and particle weight. When the light intensity was higher than the size-dependent critical intensity, all the micromotors moved away from the light source in the Z-axis direction while the “catalytic cap” was facing down. Furthermore, the small-size micromotors could hover above the bottom of the solution with low-intensity light while the large-size micromotors sided and hovered under medium and low light intensity (Figure 4d). This simple strategy demonstrated the potential to flexibly adjust the light intensity to regulate the 2D/3D motion of particles and to separate the polydisperse mixture of multisize active particles. Recently, Pumera and co-workers reported a magnetically controlled one-end open tubular $\text{TiO}_2/\text{Fe}_3\text{O}_4/\text{CdS}$ photocatalytic micromotor with six degrees of freedom (6-DoF).^[35] Three types of micromotors with different compositions were fabricated and their motion performance was systematically compared, i.e., CdS/ZnO , $\text{TiO}_2/\text{Fe}_3\text{O}_4/\text{CdS/ZnO}$, and $\text{TiO}_2/\text{Fe}_3\text{O}_4/\text{CdS}$ micromotors (Figure 4e). The $\text{TiO}_2/\text{Fe}_3\text{O}_4/\text{CdS}$ micromotors exhibited a fast photoresponsive motion and excellent degradation of nitroaromatic explosives and dye contaminants. The motion behavior of the micromotors was modulated by the simultaneous action of three forces, namely buoyancy, gravity, and a force driven by an externally visible light irradiation without any additional fuels (Figure 4f). Due to their varying components and structures, the mass and centroid position of each type of swimmer displayed distinct motion behavior. $\text{TiO}_2/\text{Fe}_3\text{O}_4/\text{CdS}$ micromotors displayed the lowest weight and its center of mass was the closest to the smaller end of the tubular structure. The oblique upward driving force produced by the photocatalytic reaction combined with the buoyancy of the micromotor balances gravity, resulting in motion in the Z-axis with 6-DoF. Conversely, CdS/ZnO and $\text{TiO}_2/\text{Fe}_3\text{O}_4/\text{CdS/ZnO}$ micromotors are heavier and only could swim at the bottom of the solution, showing the same motion behavior as other commonly reported light-driven micromotors with 4-DoF.

In a subsequent study, the same group reported the use of light-driven MXene-derived $\gamma\text{-Fe}_2\text{O}_3/\text{Pt/TiO}_2$ micromotors with 6- or 4-DoF to trap and detect microplastics efficiently.^[36] The MXene-derived $\gamma\text{-Fe}_2\text{O}_3/\text{Pt/TiO}_2$ micromotors were fabricated by thermal annealing of exfoliated $\text{Ti}_3\text{C}_2\text{T}_x$ microparticles in air at $550 \text{ }^\circ\text{C}$ to form MXene-derived TiO_2 microparticles, followed by functionalized with Pt layer deposition and $\gamma\text{-Fe}_2\text{O}_3$ nanoparticle decoration to provide light-driven fuel-free motion and fast magnetic collection. Intriguingly, micromotors exhibit two distinct types of motion behavior. Specifically, 60% of the micromotors exhibit “2D motion,” while the remaining 40% exhibit “3D motion.” This behavior is attributed to the photocatalysis of the micromotors under UV light (Figure 4g). The “2D motion” behavior is explained by the combined effects of light-driven force and buoyancy, which are not enough to counteract the gravity of the micromotor itself, and confine the motion within the XY-plane. The large electrochemical potential difference between the titanium dioxide particles derived from MXene and the platinum electrode resulted in a more powerful 2D motion than other fuel-free semiconductor-based micromotors.^[11d,28a,b] The researchers also observed that when the incident UV light comes from the bottom of the solution, the micromotor moves

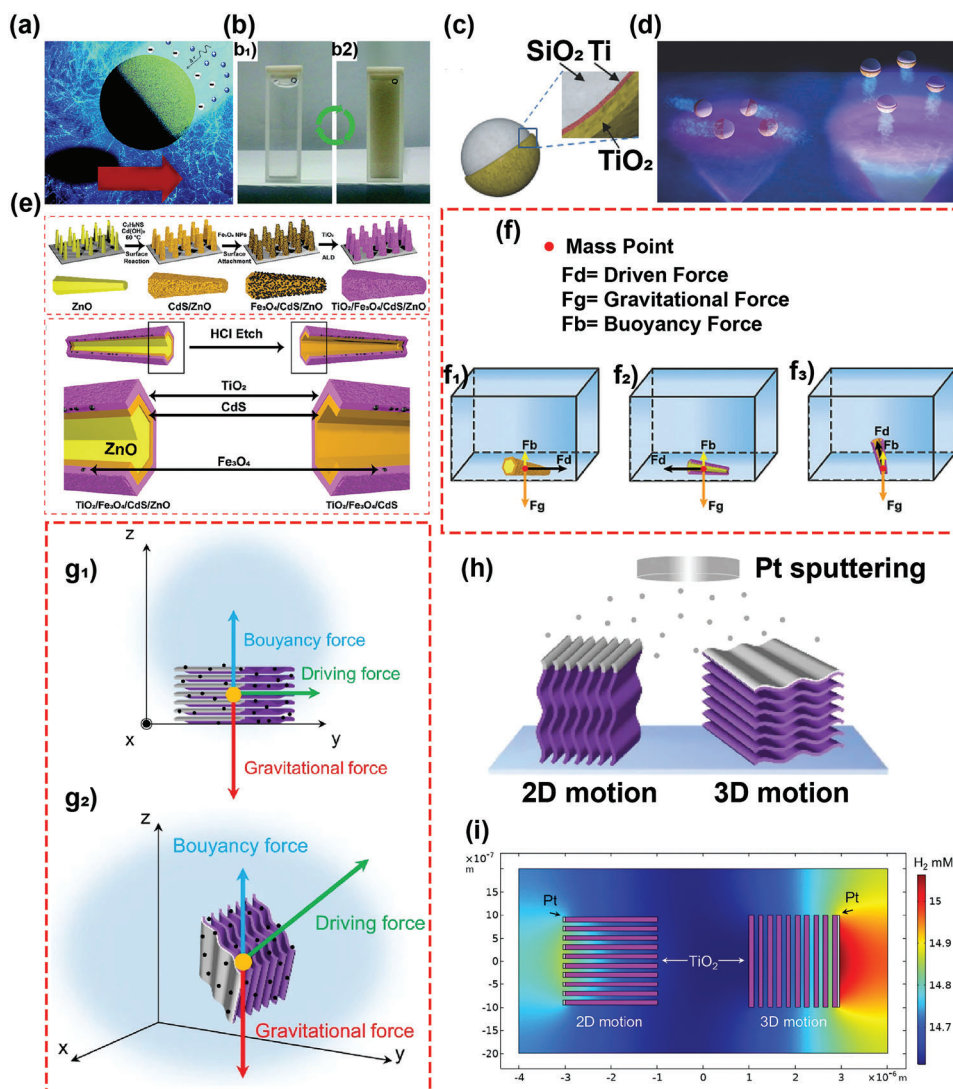


Figure 4. 3D motion of MNMs based on photocatalytic reaction. a) Schematic illustration of the phototactic movement of Pt-g-C₃N₄ micromotor. b) Digital photographs illustrate the change in solution transparency caused by micromotors b₁) before and b₂) after light irradiation. Reproduced with permission.^[30] Copyright 2017, Royal Society of Chemistry. c) The schematic diagram illustrates the multilayer structure of Janus micromotor based on spherical silica particles. d) Schematic illustration of photochemically active Janus micromotors performing 2D and 3D motion under low-intensity and high-intensity light, respectively. Reproduced with permission.^[33] Copyright 2018, Wiley-VCH GmbH. e) Schematic drawing summarizing the preparation of CdS/ZnO, TiO₂/Fe₃O₄/CdS/ZnO, and TiO₂/Fe₃O₄/CdS. f) The force analysis diagrams of three kinds of micromotors motion in the water. From left to right are f₁) CdS/ZnO, f₂) TiO₂/Fe₃O₄/CdS/ZnO, and f₃) TiO₂/Fe₃O₄/CdS/ZnO, respectively. Reproduced with permission.^[35] Copyright 2021, Wiley-VCH GmbH. g) Force Analysis of γ -Fe₂O₃/Pt/TiO₂ micromotors with g₁) 2D or g₂) 3D motion. h) The γ -Fe₂O₃/Pt/TiO₂ micromotors perform 3D or 2D motion depending on whether the deposited Pt layer is a continuous phase during fabrication. i) Numerical simulation of the spatial distribution of H₂ concentration produced by a cross-section of a micromotor motion in 2D or 3D in 0.1 s. Reproduced with permission.^[36] Copyright 2022, Springer Nature.

away from the light source in the Z-axis direction, thus exhibiting 3D motion features. This motion behavior was also similar to visible-light-driven TiO₂/Fe₃O₄/CdS micromotors discussed earlier in this section. The combination of visible-light-driven force and buoyancy was sufficient to counteract gravity, allowing the micromotor to self-orient and move with 6 DoF. Particularly, the micromotors showed a higher motion ability in 3D motion with an average speed of $16 \pm 8 \mu\text{m s}^{-1}$, compared to an average speed of $9 \pm 4 \mu\text{m s}^{-1}$ when swimming in 2D. The researchers provided further insights into the

behavior of the micromotors with 2D or 3D motion. It was noted that prior to the deposition of Pt NPs by the sputtering technique, MXene-derived TiO₂ microparticles were randomly deposited on the glass slides. This resulted in the MXene-derived TiO₂ microparticle having a continuous Pt coating on the plane or a discontinuous Pt coating on the multilayer side (Figure 4h). Consistent with previously reported studies,^[28a,29c,37] micromotors with a continuous Pt coating exhibit enhanced 3D motion. Under UV light irradiation, the H₂ evolution reaction generated at the TiO₂ side was higher than on the Pt

side, thereby establishing a larger concentration gradient of H^+ (Figure 4i).

Light-driven MNMs have received extensive attention in research, finding diverse applications in different fields. Generally, both photothermal and photochemical effects could be utilized to achieve the 3D motion of light-driven MNMs with distinct modulation mechanisms. In the case of photothermally driven MNMs, the force generated by fluid convection owing to the temperature gradient is large, and the ionic tolerance is high. However, precise modulation of their motion behavior (strength and direction) through the applied light is challenging. Besides, there is a significant motion delay in switching on and discontinuing the light-induced motion. Hence, photothermally driven MNMs are more suitable for environmental applications. Besides, the photothermal effect can also lead to bubble formation while allowing for control over their dimensions. The force driven by the generated bubbles (i.e., buoyancy) offers a way to primarily regulate the vertical motion through light power density. In addition, NIR light is widely used for noninvasive optical diagnosis and phototherapy in the biomedical field. Hence, the combination of photothermally driven MNMs, photothermal therapy, and hyperthermia-triggered drug delivery constitutes a promising approach for several therapies. Recent *in vivo* and *in vitro* research have already shown potential.^[20a,38] For photochemically driven MNMs, the force resulting from the chemical gradient around the swimmers' surface is relatively weak and usually requires light with high energy, i.e., UV and blue light. The self-weight and buoyancy regulation would play a vital role. The use of photochemically driven MNMs in photocatalysis and photosynthesis holds promise as an energy-saving strategy that may eliminate the requirements for external mechanical stirring for enhanced mass transfer. However, a significant hurdle is the low ionic tolerance of this propulsion strategy, which remains a grand challenge.

2.2. Magnetic- and Acoustic-Field-Driven MNMs

The applicability of light-powered MNMs in biological applications is somewhat limited by the damage caused by high-intensity light and the narrow window of light wavelengths available for use on biological tissues, which comprises only two regions (700–900 and 1000–1700 nm).^[39] Compared to light, acoustic and magnetic fields are more versatile for MNMs in biological applications by considering their high penetration in tissues and biocompatibility.^[40]

Magnetic forces can be generated by permanent ferromagnets or electromagnets with different coil configurations (e.g., eight-coil configuration, triaxial orthorhombic Helmholtz coils) to induce 3D motion for MNMs.^[41] Magnetic motion can be generated in two ways: a) by applying magnetic field gradients to exert magnetic forces on the MNMs and b) using dynamic magnetic fields, including oscillating or rotating magnetic fields to apply torques.^[6c,42] MNMs comprising a magnetic component with a volume v exhibit a magnetization \vec{M} and experience an attractive magnetic force \vec{F} when subject to a magnetic field gradient $\nabla\vec{B}$, as expressed in Equation (1). When subject to a magnetic field \vec{B} , the magnetic body will experience a torque \vec{T} which will cause the

MNMs to align their easy magnetization axis parallel to the direction of the applied magnetic field, as expressed in Equation (2)^[43]

$$\vec{F} = v \left(\vec{M} \times \nabla \right) \vec{B} \quad (1)$$

$$\vec{T} = v \vec{M} \times \vec{B} \quad (2)$$

Hence, the magnetically driven MNMs could be classified into magnetic-force-driven MNMs and magnetic-torque-driven MNMs. Magnetic field gradients can be directly used to realize the 3D motion of MNMs, especially in the Z-axis direction.^[41a,44] However, in most cases, the magnetic force is commonly used to steer the motion direction of MNMs powered by other energy sources, such as bubble-propelled and light-driven MNMs, because of their limited force strength against the gravitational force.^[4b,15,45] Compared to magnetic force, torques can achieve more complex motion mechanisms under low magnetic field strengths, which is an appealing feature for biomedical applications.^[43a,46]

Generally, a simple rotational motion of MNMs is not sufficient to generate a net displacement.^[35] However, when magnetic structures are manipulated close to physical boundaries, rotational motion can also be used to achieve vertical displacement. For example, a Ni nanowire can climb up and down along a vertical wall under a uniform rotating magnetic field (Figure 5a).^[47] The hydrodynamic interaction between the nanowire and the wall differs at the two ends, causing a velocity difference that generates a tumbling motion and propels the nanowire. Similarly, cell-sized multifunctional surface microrollers can move on inclined 3D surfaces due to the boundary effect (Figure 5b).^[48] Another recent research has shown that reconfigurable magnetic trimer-like microrobots under a rotating magnetic field can ascend along a vertical boundary through tumbling motion. This enables the swimmer to effectively overcome obstacles due to an increased climbing force caused by the friction between the microrobot and the surface of the vertical boundary, effectively counteracting gravity (Figure 5c).^[49] However, the 3D motion generated relying on boundaries/interfaces has practical limitations, as MNMs require the interaction with solid boundaries in order to increase the climbing force against gravity, facilitating vertical motion.^[50] Therefore, it is crucial to clarify that the scope of the 3D motion discussed in this review is limited to free-moving MNMs and excludes those that rely on boundaries/interfaces for their motion.

The first demonstration of a microscopic artificial swimmer driven by rotational magnetic fields could be traced back to 2007 by Nelson and co-workers.^[51] A key element in this design is the helical tail, which converts rotational motion into corkscrew-like translational motion, as depicted in Figure 6a,b.^[52] By simply reversing the rotation direction of the external rotation magnetic field, i.e., clockwise or anticlockwise, the forward and backward motion of the helical MNMs can be switched. In this prototype, the motion direction was controlled by the misalignment angle between the magnetic field and the thin magnetic head, generating a magnetic torque. Additional torque-driven MNMs with various structures, such as helices, screws, or twists, have been reported to move individually or in swarms in 3D space through nonreciprocal motion induced by a low-strength rotating

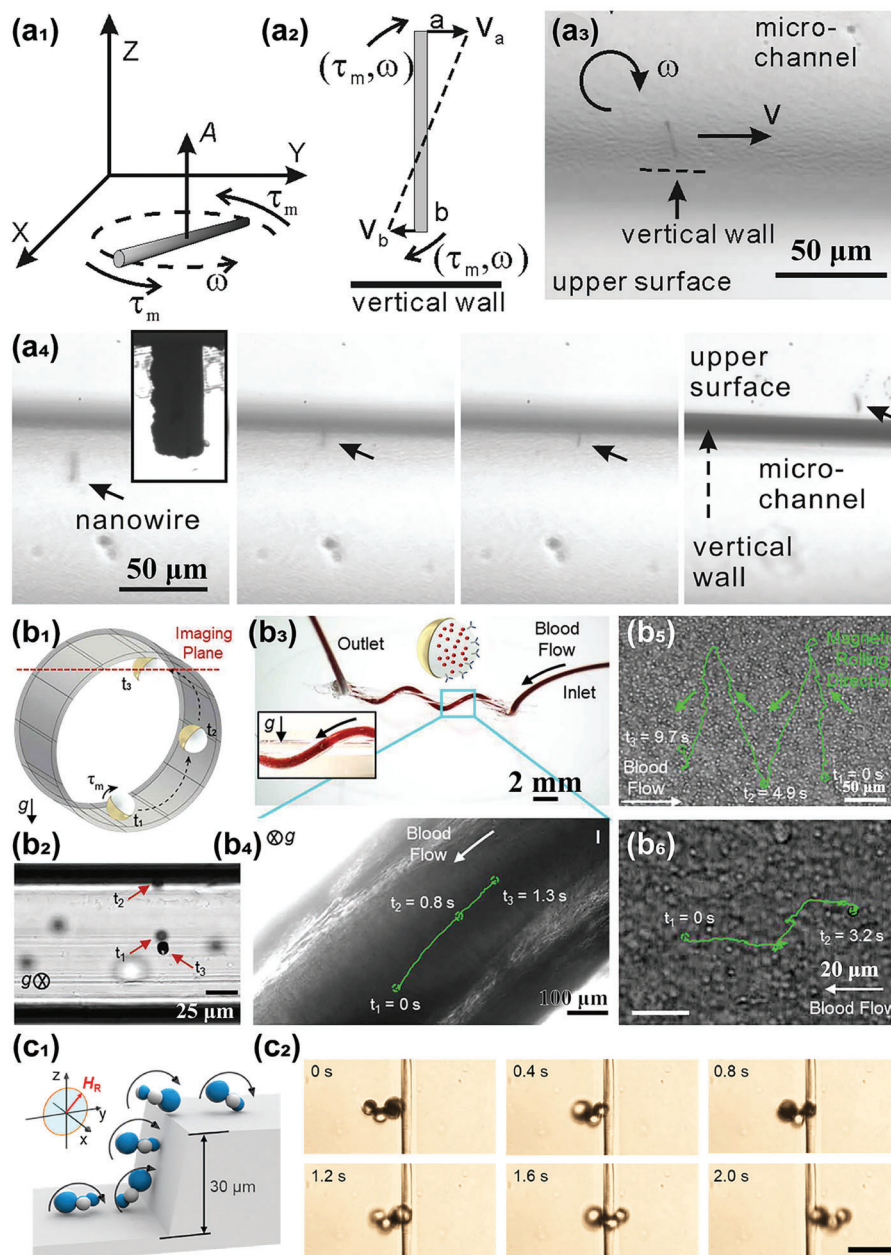


Figure 5. Vertical displacement of MNMs under rotation magnetic field relying on boundaries. a) Nickel nanowires vertically move near a patterned solid surface. Schematic showing a₁) a nanowire rotating horizontally in the X–Y-plane in the absence of boundary and a₂) the velocity difference at the two ends of the nanowire, a₃) frame exported from a video indicating the propulsion of a nanowire near a vertical wall, a₄) time-lapse images showing the upward propulsion of nanowire through a microchannel. Reproduced with permission.^[47] Copyright 2010, American Chemical Society. b) Locomotion of microrollers in 3D surfaces in static conditions and under blood flow. b₁,b₂) A microroller climbs in a cylindrical tube through the curved wall and reaches the top of the tube. *g* indicates the gravity direction. b₃,b₄) Upstream propulsion of the microroller in vitro 3D microfluidic system mimicking real blood flow conditions. b₅) Controlled triangle trajectory of the single microroller in blood flow. b₆) Upstream propulsion of the microroller on endothelialized channels in blood flow. Reproduced with permission.^[48] Copyright 2020, AAAS. c) A trimer-like microrobot overcoming an obstacle. c₁) Schematic illustration showing the microrobot climbing behavior as it navigates over a boundary. c₂) Time-lapse optical images indicate the climbing process of the microrobot overcoming the obstacle. Reproduced with permission.^[49] Copyright 2022, Elsevier.

magnetic field (Figure 6c–e).^[43a,52b,53] The initial approach for fabricating helical MNMs was through traditional thin-film deposition methods and monocrystalline thin-film growth combined with photolithography.^[52a] Later, other methods were developed, including physical vapor shadow growth via glancing angle depo-

sition, electrochemical deposition on a template, microfluidics, and biotemplating.^[54] For example, magnetically driven helical MNMs made of biotemplated MoS₂ were reported to be operated in the Z-axis when exposed to a magnetic field gradient in combination with low-strength rotating magnetic fields, and

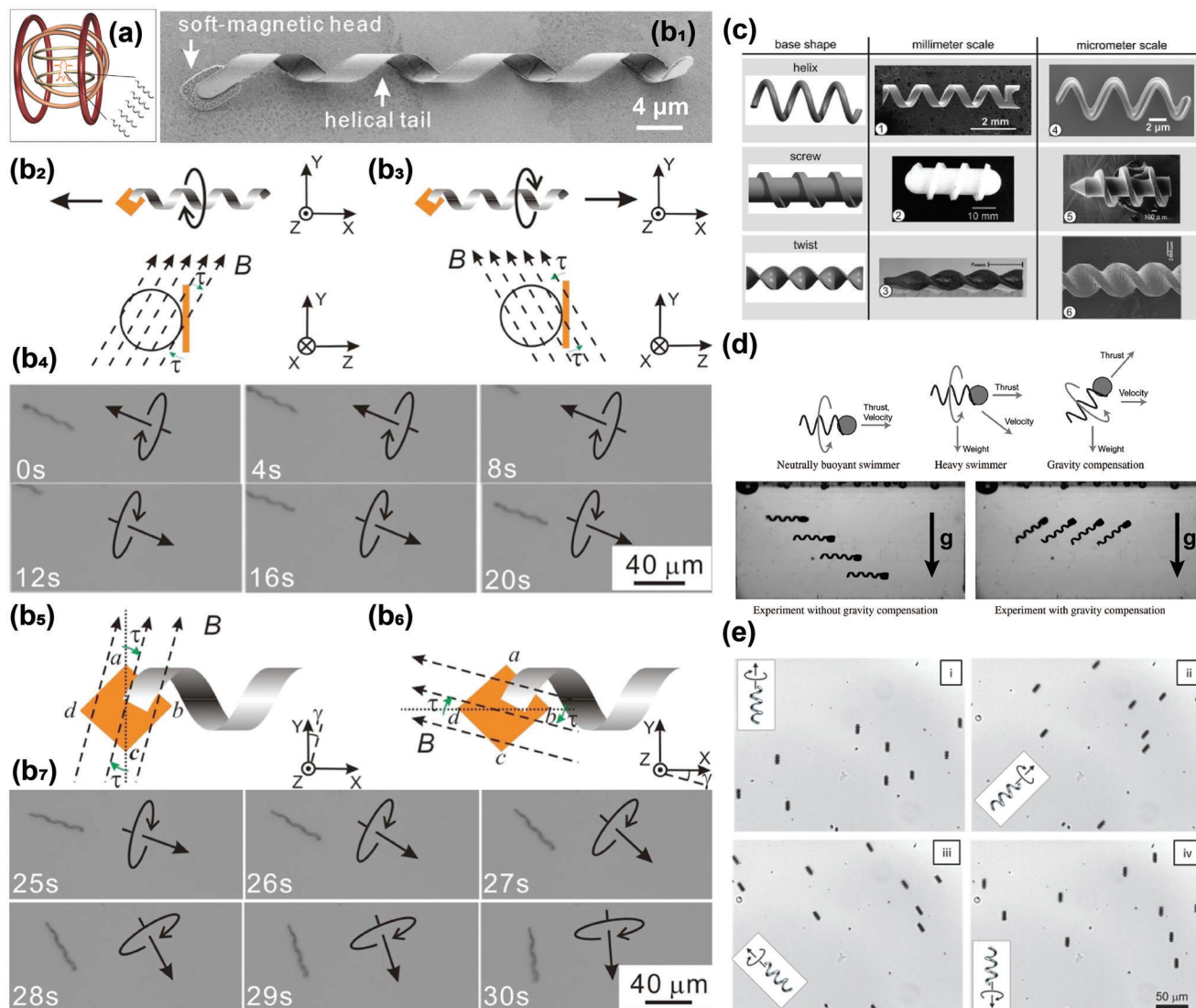


Figure 6. Vertical propulsion of MNMs under rotation magnetic field based on its helical structure. a) Scheme of triaxial orthorhombic Helmholtz coil to generate rotation magnetic field. Reproduced with permission.^[52b] Copyright 2015, Wiley-VCH GmbH. b) Helical artificial bacterial flagella (ABF) under magnetic fields. b₂, b₃) Schematic illustrating the forward and backward of a left-handed ABF swimming and b₄) the corresponding time-lapse optical microscope images. Schematic illustrating the motions b₅) attempts to align with the field or b₆) the rotate perpendicular to the helix axis respecting to the y , and b₇) the corresponding time-lapse optical microscope images. Reproduced with permission.^[52a] Copyright 2009, AIP Publishing. c) Basic shapes that can translate rotary to translation motion at different scales. Reproduced with permission.^[53a] Copyright 2013, Wiley-VCH GmbH. d) Gravity compensation of swimmers at different conditions and their corresponding time-lapse motion images. Reproduced with permission.^[53c] Copyright 2011, Taylor & Francis. e) Time-lapse optical images illustrating the controlled vertical swarm of f-ABF. Reproduced with permission.^[52b] Copyright 2015, Wiley-VCH GmbH.

demonstrated highly effective antitumor properties.^[55] Similar to other magnetically driven MNMs systems, the velocity and trajectory of MNMs strongly depend on the frequency of the applied magnetic field. More recently, direct laser writing and e-beam evaporation have emerged as a simple, general, and scalable method for fabricating helical swimmers capable of 3D directional motion under rotating magnetic fields.^[12a,56]

Oscillating magnetic fields have also been employed to provide locomotion to magnetic micro- and nanostructures. Using this approach, three main locomotion mechanisms have been identified: traveling-wave-, surface-walker-, and scallop-like propul-

sion. For more details on these motion mechanisms, the reader is referred to an extensive review on this topic.^[57] Yet, it is interesting to note that some swimmers propelled by oscillating magnetic fields capitalize on asymmetric shape deformations of their bodies to be able to propel in fluids. Recent investigations have shown that oscillating magnetic fields could be used to propel swimmers against gravitational forces. For example, Sun and co-workers have recently shown that magnetic particles exposed to a dual-axis oscillating magnetic field can self-assemble into reconfigurable vertical aggregates and overcome gravity, enabling them to navigate obstacles and climb (Figure 7a–c).^[58]

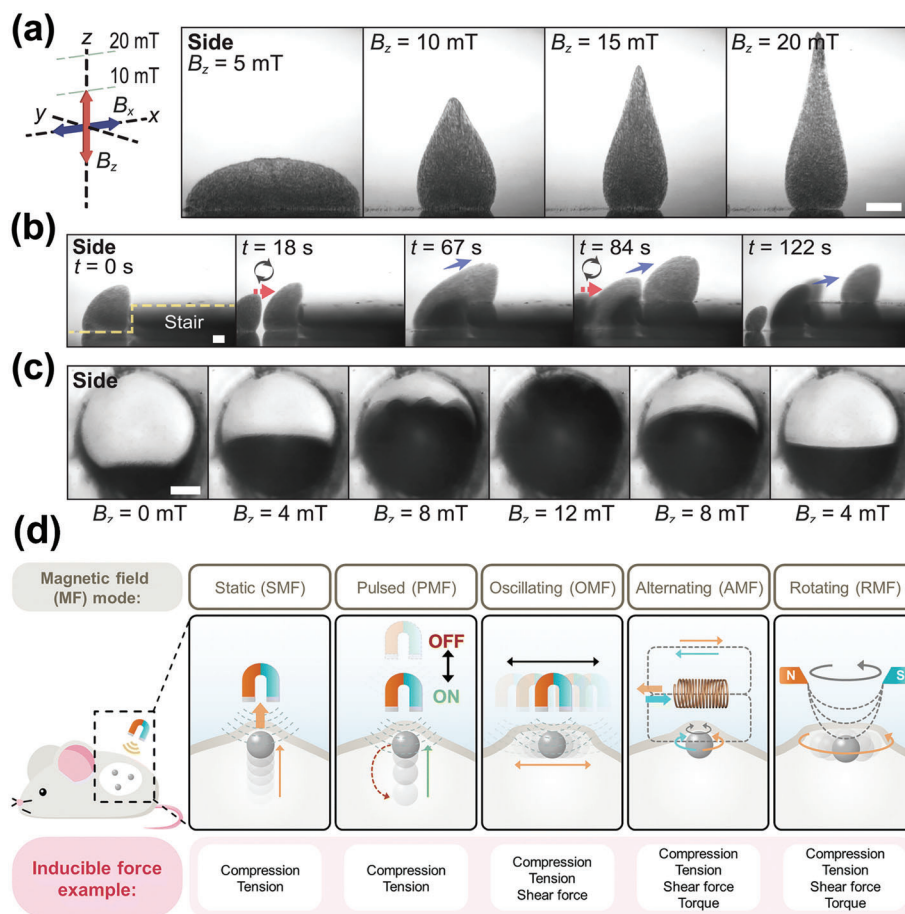


Figure 7. a–c) Vertical motion of MNMs under oscillating magnetic fields based on swarming behavior. a) The colloid collectives exhibit vertically reconfigurable behavior under different magnetic field intensities. Time-lapse optical images indicate the ability of colloid collectives b) climbing up a step and c) tuning the light path in the channel. Reproduced under the terms of the CC-BY license.^[58] Copyright 2022, AAAS. d) Schematic illustration of the precise therapy in vivo by tuning the external magnetic field modes to match the desired motor behavior of the MNMs. Reproduced with permission.^[64] Copyright 2022, Royal Society of Chemistry.

Magnetic MNMs can exhibit a wide range of locomotion behaviors that can be controlled noninvasively through remote regulation of magnetic field gradients, rotating and oscillating magnetic fields, or their combinations. Several mechanisms, such as translational rolling, precession, corkscrew, wobbling, tumbling, and undulation, can be achieved at low rotational or oscillating magnetic field strengths, making MNMs highly promising for biomedical applications.^[6c,42,59] In addition to motion control, magnetic fields can be utilized for other functionalities, such as magnetic hyperthermia, which has shown promise in advanced cancer therapy.^[60] Therefore, it would be intriguing to design a micromachine capable of generating magnetic hyperthermia therapy and also moving by switching its motion with different magnetic inputs. This entails using high-frequency alternating magnetic fields (hundreds of kilohertz) for inducing magnetic hyperthermia,^[61] while static magnetic fields, low-frequency oscillating magnetic fields (2–80 Hz),^[62] low-frequency rotating magnetic fields (0.5–130 Hz),^[63] or their combinations induce 3D motion.^[6c,43] This concept would be appealing in biomedical applications, especially in stimuli-driven cancer therapeutics (Figure 7d), as suggested in a recent

review.^[64] With their both rich functionalities and 3D motion abilities, magnetically driven MNMs have the potential to offer a wealth of biomedical applications, such as targeted delivery,^[65] accelerating thrombolysis,^[66] toxin detection,^[67] and biofilm elimination.^[68]

Acoustic propulsion has recently emerged as an interesting approach for propelling MNMs in biomedical applications, as acoustic waves are biocompatible with human tissues in a wide range of frequency and power conditions. The noncontact absorption, scattering, or reflection of acoustic radiation energy by MNMs will cause a series of self-propulsion behaviors when powered by external standing or traveling acoustic waves.^[10c,69] Generally, the force induced by a standing-wave field is relatively large. The force F is directly proportional to the volume V of the particle and to the pressure amplitude p_0 , and is expressed as (Equation (3)).

$$F = - \left(\frac{\pi p_0^2 V \beta_w}{2\lambda} \right) \phi(\beta, \rho) \sin(2kd) \quad (3)$$

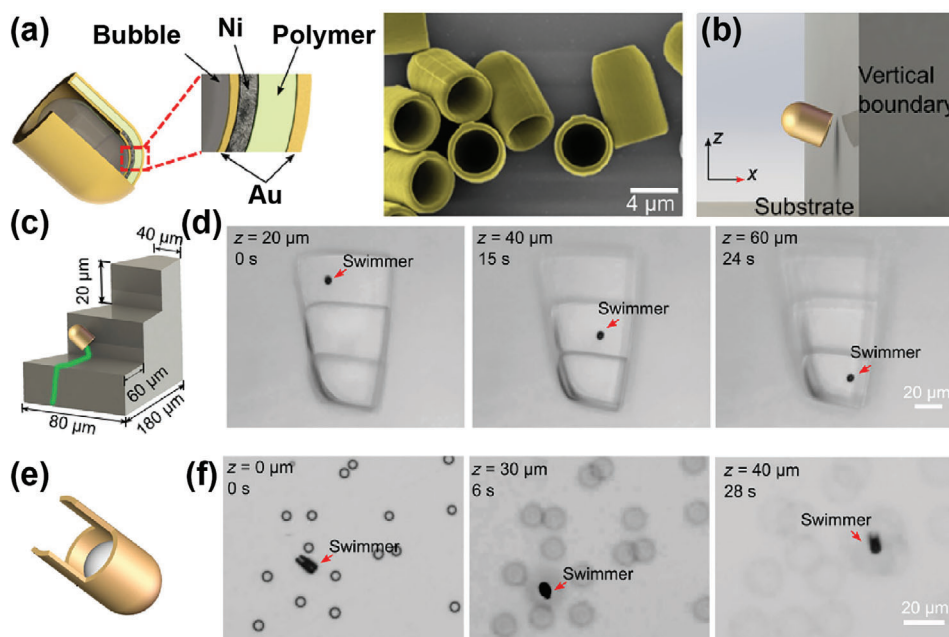


Figure 8. The 3D motion of magnetically and acoustically actuated MNMs. a) The schematic diagram and adjusted-colored scanning electron microscopy (SEM) image illustrate the multilayer hollow capsule structure of the microswimmer. b) Schematic illustrating the open end of the microswimmer automatically faces the wall boundary due to the attraction of the vertical boundary. c) Schematic illustration of the climbing behavior of the microswimmer on the three-step staircase and d) the corresponding time-lapse images. e) Illustration of the morphology-optimized microswimmer with twin tails and f) its free 3D swim. Reproduced with permission.^[14c] Copyright 2019, AAAS.

where k is the wavenumber, λ is the wavelength, and d is the distance between the particle and the node or the antinode of acoustic pressure. Additionally, the term $\Phi(\beta, \rho)$ represents the relationship between the density ρ and compressibility β of the particle and the medium, also determining the direction of the force F to be used to control the motion of the particle.^[70]

Taking into account all of the above, incorporating magnetic and acoustic control into MNMs design is a promising strategy for dual actuation, especially for motion in 3D space. Recent studies have demonstrated the 3D motion behavior of MNMs powered by ultrasound and magnetic fields.^[14c] One example of this is the capsule-shaped MNMs that researchers fabricated using 3D direct laser lithography and metallic layer deposition (Figure 8a). The surface of the micromotors was treated to become hydrophobic, which allowed them to trap an air bubble inside their inner cavity through the open end when submerged in water. Because of their hydrophobic surface, the swimmers floated on the fluid. To regulate the buoyancy and cause the swimmers to sink to the bottom of the container, a deposited gold coating was incorporated. Additionally, a magnetically responsive nickel layer enabled external magnetic fields to act as motion-actuated switches and speed controllers. Under low-power external acoustic fields, the micromotors displayed self-rotation and translational motions. Interestingly, the micromotor exhibited rich locomotion behaviors in complex 3D environments and could overcome obstacles by climbing vertical boundaries (Figure 8b). When the micromotor approached the vertical boundary, it experienced attractive forces from both the vertical boundary and the horizontal substrate. As a result, it immediately rotated to face its open end with the vertical boundary

and then moved under the guidance of the magnetic field. To demonstrate the excellent 3D motion capabilities of the micromotor (Figure 8c,d), researchers used a 3D-printed microstaircase as an obstacle. However, due to the interface attraction, the simple capsule-structured micromotors had limited 3D motion near solid boundaries. An in-depth analysis showed that increasing the distance of the air bubble inside the capsule from the boundary helped suppress this attraction. Interestingly, the introduction of a pair of small tails at the open end of the micromotor demonstrated that this improved design allows the micromotor to freely swim in any direction in 3D space without being affected by the attractive force of the substrate interface (Figure 8e,f).

The field of biomedical MNMs powered by magnetic fields or ultrasound remains still in its infancy. The combination of the acoustic and magnetic fields to control the 3D motion of the MNMs is also interesting, although it requires high-level external equipment, which becomes challenging for practical applications. Nonetheless, this type of MNMs stands among the most promising candidates for biomedical applications, especially in targeted drug delivery, localized surgery, and disease diagnosis.

2.3. Electric-Field-Driven MNMs

Electric fields are another alternative approach for controlling locomotion in MNMs, often referred to as electric tweezers.^[71] Studies have shown that MNMs with conductive material components can be easily actuated by constant, direct current (DC), or alternating current (AC) electric fields. The applied external electric field can induce the propulsion of the MNMs or control the

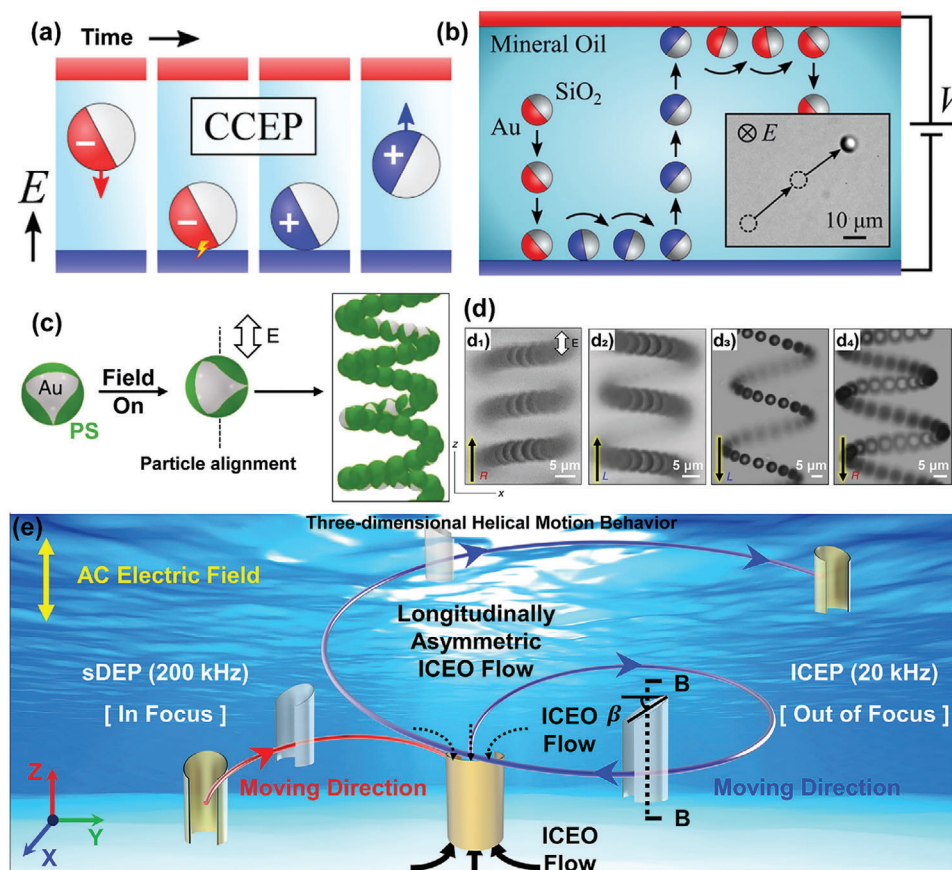


Figure 9. 3D motion regulation by an external electric field. a) Particles propelled by contact charge electrophoresis (CCEP) acquire a charge of opposite polarity when they contact one electrode. b) Schematic diagram illustrating the combination of vertical and translational rolling motion of metallodielectric Janus particles between two electrodes. Reproduced with permission.^[14d] Copyright 2016, American Chemical Society. c) Schematic illustration of the initial alignment and subsequent helical motion of particles when subjected to an external alternating electric field. d) These photographs depict four distinct helical trajectories of particles, with R and L denoting right-handed and left-handed helical paths, respectively. The arrows indicate the direction of upward or downward movement within each trajectory. Reproduced with permission.^[14e] Copyright 2016, Springer Nature. e) Schematic illustration showing the 3D helical motion behavior of longitudinally asymmetric defective golden micro-/nanomotors under an AC electric field. Reproduced with permission.^[75] Copyright 2021, Elsevier.

direction of motion by adjusting the surface charge of the MNMs or inducing an electrochemical reaction at the interface.^[72]

Research has shown that the motion of conductive particles in insulating liquids was driven by contact charge electrophoresis (CCEP). In CCEP, the particles come into contact with an electrode, acquire a charge of opposite polarity, and subsequently migrate toward another electrode, effectively transferring the charge along the applied potential gradient.^[73] In 2016, Bishop and co-workers demonstrated that the Z-axis motion of the metallodielectric Janus particles could be regulated by applying two parallel electrodes.^[14d] The SiO₂@Au conductive particles were immersed in electrically insulating mineral oil and rapidly oscillated between an electrode array comprising perpendicularly aligned top and bottom electrodes, all under a constant voltage. Additionally, both theoretical and experimental evidence confirmed that the particles near the electrode surface displayed a horizontal rolling displacement in the plane caused by the field-induced rotation. When the metal side of the particle is oriented away from the nearest electrode, it will be propelled in the Z-axis direction toward the metal side until the particle comes into contact with

another electrode, allowing for the steady cycle of lateral and vertical displacement to continue (Figure 9a,b).

Applied AC electric fields are an alternative method for the oriented motion of particles, which is based on induced charge electrophoresis (ICEP) and particle asymmetries.^[74] Bharti and co-workers prepared metallodielectric particles with triangular metal patches by physical vapor deposition of chromium and gold layers on the surface of polystyrene (PS) microspheres, demonstrating that the particles can be driven by an AC electric field to move along spiral trajectories on the Z-axis (Figure 9c).^[14e] By adjusting the switch of the AC electric field, the particles exhibited four different motion states, i.e., negative Z- or positive Z-axis direction and right- or left-handed helical trajectory (Figure 9d), depending on the initial orientation of the particles when the AC electric field was applied. Interestingly, the difference in the metal patch area on the surface of the PS microspheres will lead to a change in the radius of the spiral trajectory in the field. By contrast, the strength of the applied electric field will only affect the particle's speed. Recently, Li and co-workers showed that defective golden micro-/nanomotors displayed controllable

self-dielectrophoresis and ICEP motion behaviors under AC electric fields. In particular, a 3D helical motion behavior could also be achieved with longitudinally asymmetric defective golden micro-/nanomotors (Figure 9e).^[75]

The precise manipulation of MNMs, including their position, speed, orientation, and assembly, can be achieved by means of electric tweezers using a combination of AC and direct DC electric fields. This approach holds promise for advanced applications in biology, such as in vitro biomolecule delivery to individual cells, biocargo transportation, and tunable biomolecule release.^[76] Additionally, the rotational behavior of MNMs can be realized by employing external high-speed rotational electric fields. This strategy can be used to enhance the capturing and sensing capabilities of dilute biomolecules suspended in a solution, which holds promise for applications in disease diagnosis protocols.

3. New Strategy and Potential Approaches for Vertical Motion

Currently, there are few reported approaches for the vertical motion of MNMs. The typical artificial flagellar-based MNMs present poor motion capabilities in the Z-axis direction, making it challenging to maintain their suspension at varying depths when the external field is withdrawn. By contrast, some organisms in the natural world control their Z-axis movement through buoyancy regulation. For instance, bacteria employ gas vesicles, while fish rely on air bladders. The regulation of vertical motion through buoyancy, achieved by generating bubbles, is significantly different from the vertical motion of MNMs propelled by bubble recoil. In the latter, generated bubbles attach to the surface and regulate the vertical motion behavior through volume adjustment in response to the external environment. Although the buoyancy-regulation-based vertical movement approach has been utilized by a few swimmers larger than a centimeter, its use in the area of MNMs remains unexplored.

The bubble-based buoyancy regulation technique was initially applied to centimeter-scale devices to achieve vertical motion manipulation. Since 2010, Shi and co-workers have performed a series of research by integrating a stimulus-responsive polymer coat and a bubble generator to achieve a diving-surfacing cycle to mimic a submarine.^[77] Specifically, a functionally cooperating system, based on a pH-responsive surface (a mixture monolayer of 1-decanethiol and 11-mercaptopundecanoic acid (SH(CH₂)₉CH₃/SH(CH₂)₁₀COOH)) and hydrogen-peroxide-responsive platinum (Pt/H₂O₂), was designed to experience a pH-stimulus diving-surfacing cycle.^[77a] Upon changing the solution from acidic to basic, the surface will undergo a pH-responsive transformation from superhydrophobicity to superhydrophilicity, causing the smart device to dive. Conversely, by adding H₂O₂ and causing the pH of the solution to revert back to an acidic state, the smart device can rise and resurface due to an increase in buoyancy caused by the surface bubble adhesion. Similarly, another two systems with a cooperative functionality were designed: one comprising a thermally responsive surface (poly(*N*-isopropylacrylamide) and Pt/H₂O₂,^[77b] and the other entailing a pH-responsive surface (a mixture monolayer of SH(CH₂)₉CH₃/SH(CH₂)₁₀COOH) and an acid-responsive hydrogen bubble generator (Mg/HCl).^[77c]

The hydrophobicity/hydrophilicity transformation of the thermally responsive component and the pH response of the bubble generator are critical elements for controlling the bubble adhesion in these functionally cooperating systems. Based on this system, several stimuli-responsive smart devices have been developed. Pan and co-workers realized a smart miniature submarine system moving at various air/liquid or oil/water interfaces, where the surface coating carboxyl-terminated poly(2-(diethylamino)ethyl methacrylate exhibited a CO₂-responsive wettability switch (Figure 10a).^[78] In 2021, Chen and co-workers were inspired by a diving beetle and conceived a novel concept of underwater adhesion to realize repeatable particle manipulation and particle self-assembly, which functioned across a wide variety of scales.^[79] In this system, the air bubble is initially trapped in the nontilt cone array surface. In the future, an underwater adhesion/repulsion regulation approach based on bubbles and engineered surfaces may be developed to control the MNMs' diving and floating behavior observed in diving beetles.

In addition to the approaches of buoyancy regulation via surface bubble adhesion using stimuli-responsive polymer coatings and bubble generators, NIR light is another versatile method. Photothermally induced convection is the main force powering the vertical motion in MNMs. However, the use of NIR light is more promising in centimeter-scale devices. Du and co-workers designed a NIR-light-driven controllable centimeter-scale device based on the gold-hollow-microcone array.^[80] The excellent plasmonic heating property of the Au hollow microcone array can generate vast amounts of vapor bubbles in a liquid upon NIR light irradiation. Photothermally induced convection coupled with the generated vapor bubbles can drive the reversible floating and diving motions of the integrated centimeter-scale device by switching on and off NIR. Furthermore, the NIR-driven photothermal conversion could be used to regulate trapped air bubbles and drive the horizontal motion of a motor, its suspension, and also its vertical movements underwater.^[81] Deng and co-workers designed a NIR-responsive motor based on the above motion regulation mechanism. The researchers attached two polydimethylsiloxane-coated oxidized copper foams (POCFs) to the two opposite sides of an oxidized copper foam. When immersed in water, the hydrophobic POCF could serve as both an air bubble trapper and a light-to-heat conversion center. The volume of trapped air bubbles could expand or contract in response to temperature, resulting in behaviors such as diving, floating, and suspension (Figure 10b).

In addition to the conventional approach of using self-storage of air bubbles or generating them via chemical or physical triggers, an alternative method involves directly converting low-boiling-point liquids into gas at significantly low temperatures. Recently, this strategy has been reported with a proof-of-concept inflatable system comprising a soft body made of a shape-memory polymer (Ecoflex elastomer matrix) infused with a low boiling point liquid (Novac 7000, with a boiling point of around 34 °C). Magnetic particles (Fe₃O₄ nanoparticles) were incorporated into the polymer for remote heating by means of radiofrequency (RF) magnetic field.^[82] Upon the application of a remote RF magnetic field, Fe₃O₄ NPs enabled the heating of the liquid phase, which in turn, triggered the inflation of the system

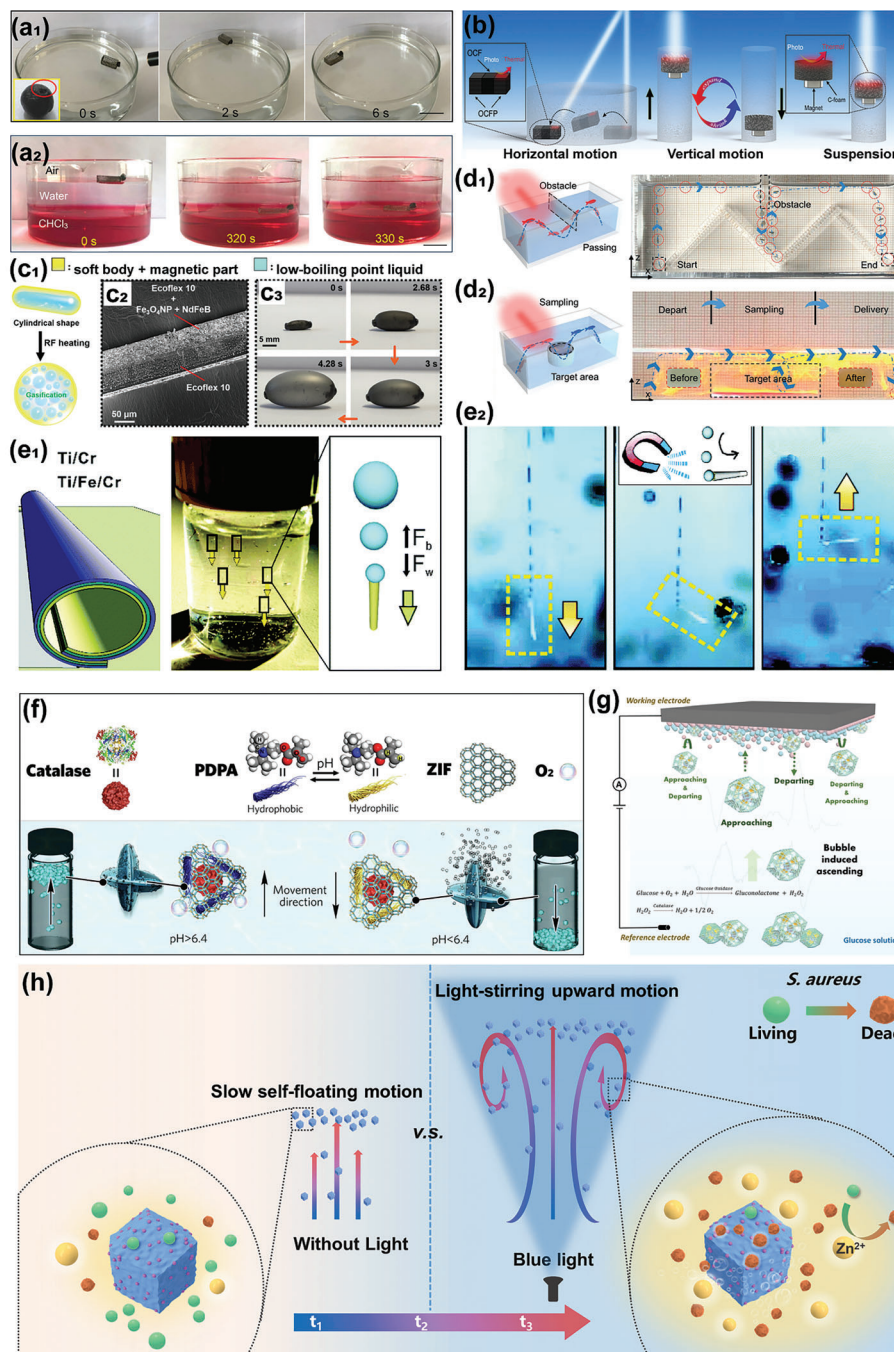


Figure 10. Potential approaches to facilitate 3D motion of MNMs. Digital photographs show the minisubmarine's motion a₁) at the water surface, and a₂) water/CHCl₃ interface. Reproduced with permission.^[78] Copyright 2018, American Chemical Society. b) Under NIR irradiation, the small motor causes the volume change of the internal air bubble to show three different motion modes: translation, vertical, and suspension. Reproduced with permission.^[81] Copyright 2019, Wiley-VCH GmbH. c) Phase-change magnetic soft body with inflation behavior. c₁) Schematic of volume inflation of soft magnetic body under magnetic-RF heating, c₂) SEM image of the soft magnetic body showing a composite bilayer film configuration, and c₃) time-lapse photographs of the corresponding inflation process. Reproduced under the terms of the CC-BY license.^[82] Copyright 2022, Wiley-VCH GmbH. d) 3D motion of motor driven by NIR and its application. d₁) Pass through an obstacle, d₂) sample the target area and perform transportation tasks. Reproduced with permission.^[83] Copyright 2021, Wiley-VCH GmbH. Buoyancy-regulated MNMs through the surface generation of carbon dioxide microbubbles in carbonated water e₁) in the absence of magnetic field and e₂) under a magnetic field. Reproduced with permission.^[85] Copyright 2018, Royal Society of Chemistry. f) ZIF-L-based micromotors encapsulated with catalase and PDPA exhibit ascending or descending motion at pH above or below 6.4, respectively. Reproduced with permission.^[86] Copyright 2019, Elsevier. g) Dynamic vertical motion of ZIF-8-based micromotors functionalized with catalase and glucose oxidase. Reproduced with permission.^[87] Copyright 2022, Wiley-VCH GmbH. h) Schematic diagram showing the vertical motion and antibacterial mechanism of ZIF-8-based MOFtors. Reproduced with permission.^[88] Copyright 2023, Royal Society of Chemistry.

(Figure 10c). The reported configuration with its reversible expansion property has the potential to regulate its buoyancy within a fluid via NIR or RF heating and is used as a motor with controllable 3D motion capabilities.

Certain thermally responsive hydrogels like polymer poly(*N*-isopropylacrylamide), when placed on a liquid–air interface and exposed to a NIR laser beam, can induce changes in the surface tension of the surrounding liquid. This phenomenon, known as the Marangoni effect, enables the device to move without relying on air bubbles. Li and co-workers designed Marangoni-effect-driven actuators using a temperature-responsive hydrogel and photothermal nanoparticles, which combine the Marangoni effect with photothermal buoyancy flow for complex self-propulsion and floating/sinking motion (Figure 10d).^[83] Similarly, Song and co-workers also fabricated light-powered polyvinyl-alcohol-nanofibrous-based composite motors, which exhibited direction-controlled multimodal locomotion (vertical movement, horizontal movement, and rotation) with a maximum speed of 39 mm s⁻¹ relating to the direction of light irradiation.^[84]

Lately, in the MNM field, some works started to report the MNMs with vertical motion based on bubble-based buoyancy regulation. Solovev and co-workers presented the first example of buoyancy-regulated MNMs through the surface growth of carbon dioxide microbubbles in carbonated water and brewed beverages together with the external magnetic field (Figure 10e).^[85] Enzymatically driven MNMs can display the Z-axis motion behavior when their components are rationally engineered. For instance, Liang and co-workers synthesized zeolitic imidazolate framework-L (ZIF-L)-based submarine-like micromotors equipped with a bioactive enzyme (catalase, CAT). This enzyme catalyzes the generation of O₂ bubbles from H₂O₂. Additionally, a pH-responsive element (polymer poly(2-diisopropylamino)ethyl methacrylate, PDPA) was incorporated. PDPA acts as a pH-dependent buoyancy modulator as it can capture the generated O₂ bubbles when it is in its hydrophobic state (pH > 6.4), or release them when it becomes hydrophilic upon protonation (pH < 6.4). This cooperative assembly can efficiently regulate the micromotor's buoyancy force (Figure 10f).^[86] In a follow-up study by the same group, the ZIF-8-based micromotor was encapsulated with two enzymes, i.e., CAT and glucose oxidase (GOx). Briefly, the researchers placed the micromotors in a glucose solution, and the produced O₂ bubbles remained inside the ZIF-8 framework, causing an increase in buoyancy, thus triggering the vertical motion. Significantly, the production of O₂ bubbles could be controlled by changing the concentration of glucose in the solution. This enables a dynamic control over the Z-axis motion of the micromotors, which arose from the reactions catalyzed by GOx and CAT, where GOx consumes oxygen and CAT produces it (Figure 10g).^[87] Ying and co-workers recently designed versatile multiwavelength light-responsive MOFtors through in situ encapsulation of polypyrrole (PPy) nanoparticles in ZIF-8 for water sterilization (Figure 10h).^[88] Under the irradiation of NIR/UV/blue light, the self-floating MOFtors (PPy/ZIF-8) exhibited negative phototaxis and high-speed motion behavior with a strong 3D movement. The light irradiation could accelerate the upward propulsion of the MOFtors by boosting the transformation of stored gas into bubbles, as a consequence of the elevated temperature.

4. Current 3D Motion Observation and Tracking Technique

Observing and tracking the motion of MNMs is fundamental to understanding their motion behavior and manipulation abilities. For millimeter-sized or larger motors, a digital camera or even a smartphone is sufficient. Conversely, when the size of MNM scales down to the micrometer or sub-micrometer range, a conventional wide-field optical microscope is typically the primary instrument to visualize MNMs' movement. However, the short depth of focus of the optical microscopy system, typically around 2–3 μm, creates a trade-off between the magnification and the depth of focus. This can pose significant challenges when attempting to track the motion of MNMs with vertical motion, as they may quickly move out of the focus plane, resulting in a defocused image of the swimmers. As the size of these microscopic swimmers scales down to the nanoscale, conventional microscopy is not ideal because of resolution limitations, beyond which details smaller than half the wavelength of light cannot be resolved. Nonetheless, in an optical setup, nanoparticles with dimensions below the diffraction limit can scatter incident light, which results in a radiating point, thus providing an approximate indication of their position.^[89] Commercial nanoparticle tracking analysis technology, i.e., NanoSight NS300, was widely employed in detecting and visualizing the populations of nanomotors that address the limitations of optical microscopy based on the laser scattering generated by moving particles.^[90] Additionally, in the 1990s, the stochastic optical reconstruction technique was conceived and revolutionized the imaging field by pushing the lateral resolution diffraction limit to the nanometer scale.^[91] This technique, which operates below the wavelength of light, is commonly used to study the Brownian motion of nanoparticles in water-based systems.^[92] Yet, to date, this technique has not been used to track the motion of nanomotors. In this review, we focus on the current techniques and systems used for observing and tracking micromotors.

Detecting the 2D motion of nanomotors on a plane (XY-plane) in aqueous conditions where the vertical position change approaches zero (Z = 0) is relatively straightforward. However, in a biological system, the signal-to-noise ratio decreases significantly with increasing penetration depth due to absorption and strong light scattering. To address this, Schmidt and co-workers designed an IR imaging and photoacoustic imaging system for real-time tracking of micromotors in deep tissue with high spatiotemporal resolution (Figure 11a,b).^[93] Additionally, analyzing the motion behavior of MNMs with vertical movement presents a significant challenge. When the MNMs move too far from the focus plane, defocus blur occurs. Sulzmann and Jacot developed the first high-precision tracking system to cope with the visualization, manipulation, simulation, and position of the micromotors.^[94] Based on the defocus images, Mallouk and co-workers proposed a qualitative method for analyzing vertical movement behavior.^[14c] The position change in the vertical direction (i.e., the Z-axis) was qualitatively monitored by defocusing the tracer particles at the bottom of the chamber. In addition, a height reference, i.e., a micrometer staircase with three steps (20 μm), was placed in the bulk fluid system to accurately illustrate the vertical motion of MNMs. Zhang and co-workers employed conventional microscopy for the top view and a pen-type

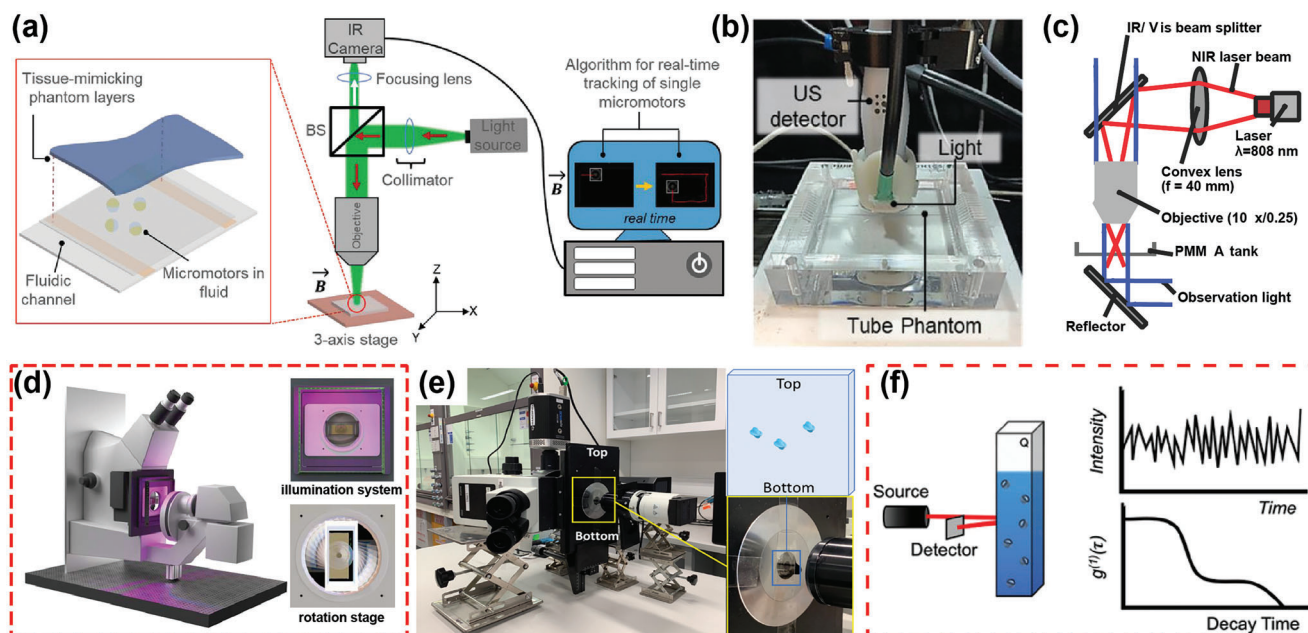


Figure 11. Current 3D motion observation and tracking techniques. Schematic diagrams of a) the IR imaging system and b) the photoacoustic imaging setup. (a) Reproduced with permission.^[93a] Copyright 2019, Wiley-VCH GmbH. b) Reproduced with permission.^[93b] Copyright 2021, Wiley-VCH GmbH. c) Schematic illustration of the construction of optical devices in the observation device, including laser (red line) and observation light (blue line). Reproduced with permission.^[21b] Copyright 2020, American Chemical Society. d) Digital photographs showing the device that turns the Olympus IX53 inverted microscope 90° to observe 3D motion freely. Reproduced under the terms of the CC-BY license.^[95] Copyright 2017, eLife Sciences Publications Ltd. e) Schematic diagram of the DLS system was used to characterize the 3D motion of the micromotor indirectly. Reproduced with permission.^[86] Copyright 2019, Elsevier. f) Motion characterization of active motion by DLS. Reproduced with permission.^[96] Copyright 2021, Wiley-VCH GmbH.

microscope (500×) set with a depression angle of 25° for the side view to simultaneously achieve a 3D motion observation (Figure 11c).^[21b] Sun and co-workers built an electromagnetic manipulation system with two movable orthogonal microscopic cameras (top-view and side-view cameras) to automatically monitor the position in the 3D space of MNMs.^[41a]

The rapid development in optical microscopy within the biological field has shed new light on solving the tracking challenges in the field of MNMs. Similarly, developmental, physiological, and cell biological studies encounter a common need, as these fields require examining vertically growing structures, such as root tips. To ease optical imaging, a confocal microscope setup was engineered, featuring a vertical sample mounting and integrated illumination (Figure 11d).^[95] With this technique and modification of optical microscopy, the Z-axis motion tracking would be possible. Liang and co-workers demonstrated the first proof by employing a 90° flipped inverted microscope and a thin glass chamber stacked with two cover glasses (Figure 11e).^[86] To minimize the side effects of image distortion and constrained motion in the XY-plane, a commercial one-end sealed borosilicate capillary microglass slide as the MNM container is a better choice for investigating vertical motion. This is a more effective alternative compared to the use of a conventional glass slide placed on top of the cover glass. This alternative container provides improved stability and confinement for the nanomotors, ensuring they move primarily in the Z-axis direction.

Similar to the widely used tracking system in nanomotors, McGlasson and Bradley employed the dynamic light scattering (DLS) system as an alternative characterization method

to investigate 3D micromotor motion in bulk dispersions (Figure 11f).^[96]

The field of motion tracking and analysis, particularly in the vertical direction, has not received much attention, and there are limited systematic studies on this topic.^[93a,94,96] Therefore, there is a need for further research to enrich the motion tracking and analysis system, with an emphasis on the vertical direction. The development of an advanced and reproducible 3D tracking system would be a significant step forward for this field.

5. Conclusions and Outlook

Over the past decade, exploratory studies of 3D motion MNMs have proved intriguing for their potential applications in biomedical and environmental fields. However, groundbreaking theoretical and experimental research on vertical movement generation and control remains unexplored. Developing MNMs that can perform complex tasks as their macroscopic counterparts (i.e., robots that are visible to the naked eye) is still challenging because of several challenges. One of the main hurdles is the lack of precise and convenient on-demand motion regulation, which hinders the swimmer's ability to perform specific movements accurately and efficiently. Additionally, operating external equipment and monitoring the swimmer's motion trajectory can be complex and time-consuming, further complicating the process. As a result, there is a need for research and innovation in areas such as motion control, sensing, and robotics engineering to overcome these challenges and develop advanced tools capable of performing complex tasks with precision and reliability. As

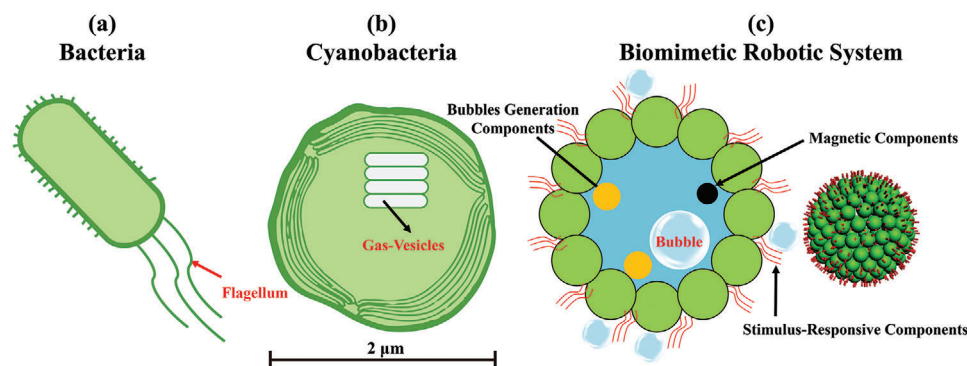


Figure 12. Two representative motion behaviors in nature: a) flagellum-propelled bacterial and b) gas-vesicle-based cyanobacterium. c) Proposed construction of a biomimetic robotic system based on a buoyancy regulation approach with multiple components, mimicking cyanobacterium's 3D motion behavior.

mentioned above, H_2O_2 -fueled bubble-propelled MNMs constitute a relatively simple strategy to achieve 3D motion, benefitting from the powerful recoil of the bubbles and a large number of different catalytic “engines” to choose from. However, there are still significant hurdles, such as short-term performance, uncontrollable directionality, stability issues, and potential side effects if one considers complex environments such as the human body or contaminated water. For example, because of the fuel consumption and self-gravity, the microplastic removal process using the bubble-propelled Fe_2O_3 - MnO_2 micromotors occurs primarily at the bottom of the container, that is, on the 2D horizontal plane. Hence, this approach is not yet optimal for capturing microplastics floating near or at the top surface of the liquid.^[97] By contrast, when considering aspects such as maneuverability and long-term navigation, externally controlled MNMs are excellent strategies to realize the movement in 6-DoF. However, while externally applied fields have advantages, it is important to consider their limitations. For example, the use of light energy is not limited by space. However, its penetration effectiveness diminishes as the solution depth increases. Additionally, aspects such as biocompatibility restrict the applicable range of light wavelengths, for example, in applications in the biomedical area. By contrast, magnetic and acoustic fields display better penetration and biocompatibility features, but the fabrication of magnetically and acoustically propelled MNMs can be complicated, and their control requires highly specialized setups and characterization methods. Another factor to consider is the limited applicability of 3D motion of nanoparticles controlled by external electric fields.

For future 3D motion MNMs, several research directions need to be explored to overcome current challenges and maximize their potential in various applications. These directions include but are not limited to the following aspects: i) further studies on the selection and matching of various components in the MNM design process are necessary, such as stress response, energy band position, density, stability, size, and ratio; it is also important to explore optimal synthetic strategies for the large-scale fabrication of MNMs, which is a current barrier faced to date, and should be overcome in the future, ii) understanding the relationship between the components/structure of the MNMs and the implementation, accuracy, timeliness, and the mechanism of its 3D motion regulation, including the inherent physicochemical reactions, surface state (hydrophilic and hydrophobic), fluid dy-

namics, bubble generation, gradient field establishment, iii) exploring ways to enhance the efficiency of MNMs in the Z-axis direction and show the potential advantages in complex environments. For instance, design concepts such as the bionic bacterial flagella using pushing forces, the incorporation of gas vesicles inspired by cyanobacteria-based buoyancy regulation, or a combination of both could be used to address current challenges in controlling the vertical motion of small-scale motile systems (Figure 12). The 3D motion capabilities of MNMs for enhancing solution mixing and achieving precise control within 3D space hold promise in several applications in environmental remediation and drug delivery. In the areas of environmental remediation and chemical synthesis, MNMs with 3D motion capabilities could mimic the behavior of cyanobacterium, which floats on the water surface or suspends at various depths in response to environmental changes. Adopting this behavior, MNMs could significantly boost the performance of photocatalytic processes through improved mass transfer efficiency, consequently enhancing the capture and adsorption of target molecules. In the biomedical field, the achievement of 3D motion and control would enable MNMs to function as miniaturized medical agents that can navigate through complex biological environments, swim through narrow vasculature, and effectively overcome obstacles present in biological fluids and barriers. Further development in the realization of these swimmers will allow these devices to reach specific lesion sites, enabling targeted drug delivery, biological sampling, medical imaging, or microsurgery. However, the observation and tracking techniques for 3D motion MNMs are still in their infancy. Therefore, another significant task for future research is to enrich these techniques and promote the perfect match between practical scientific research and external supporting equipment. This will create possibilities for wider environmental and biomedical applications of MNMs in the future.

Although 3D motion generation and control are essential aspects of MNMs, not all systems require to be precisely controlled in 3D space for their intended application. The fields of application can be divided into two areas: rapid motion in 3D space for environmental remediation and accurate motion control in 3D space for cargo delivery. In environmental remediation, fast 3D motion is crucial to enhance convection and improve adsorption or degradation. By contrast, cargo delivery requires more precise 3D motion control, although speed requirements may not be as

high. Integrating the concept of perfect 3D motion on MNMs is challenging, but it could be a valuable solution for promoting more MNMs toward real-world applications. To meet the growing demands of different fields, we need to design MNM systems with different motion speeds and control precision based on various structures and compositions. While there is still a long way to fully unlock the advantages of MNMs with 3D motion capabilities and turn them into socioeconomic benefits, we believe that considerable advances will come from the field in the next few decades.

Acknowledgements

H.H. and Y.Y. were supported by the National Natural Science Foundation of China (Grant No. 52203147), the Zhejiang Provincial Natural Science Foundation of China (Grant No. LQ22B010006), and the Science Foundation of Zhejiang Sci-Tech University (Grant No. 21212243-Y). S.Y. and L.Z. were financially supported by the Research Impact Fund (Project No. R4015-21) and the Research Fellow Scheme (Project No. RFS2122-4S03) from the Research Grants Council of Hong Kong. J.P.-L. and S.P. would like to acknowledge the ERC Consolidator Grant (CoG) HINBOTs (Grant No. 771565), the FETPROACT-EIC-05-2019 ANGIE (Grant No. 952152), and the Swiss National Science Foundation (Project Nos. 192012, 190451).

Open access funding provided by Eidgenössische Technische Hochschule Zurich.

Conflicts of interest

The authors declare no conflict of interest.

Keywords

3D motion, buoyancy, force regulation, micro-/nanoswimmers, z-axis motion

Received: June 19, 2023

Revised: September 8, 2023

Published online: November 27, 2023

- [1] R. P. Feynman, presented at Lecture American Physical Society Meeting, Caltech, December 1959.
- [2] a) J. W. Pepper, G. Hoelzer, *Science* **2001**, 294, 1466; b) M. Nagy, Z. Ákos, D. Biro, T. Vicsek, *Nature* **2010**, 464, 890.
- [3] a) H. Zhu, B. Xu, Y. Wang, X. Pan, Z. Qu, Y. Mei, *Sci. Rob.* **2021**, 6, eabe7925; b) E. Karshalev, C. Silva-Lopez, K. Chan, J. Yan, E. Sandraz, M. Gallot, A. Nourhani, J. Garay, J. Wang, *Nano Lett.* **2021**, 21, 2240; c) F. Wang, D. Huang, Q. Li, Y. Wu, B. Yan, Z. Wu, S. Park, *Compos. Sci. Technol.* **2023**, 237, 109845.
- [4] a) M. Chen, Z. Lin, M. Xuan, X. Lin, M. Yang, L. Dai, Q. He, *Angew. Chem., Int. Ed.* **2021**, 60, 16674; b) Y. L. Ying, A. M. Pourrahimi, Z. Sofer, S. Matejkova, M. Pumera, *ACS Nano* **2019**, 13, 11477.
- [5] a) T. Kudernac, N. Ruangsapapichat, M. Parschau, B. Maciá, N. Katsonis, S. R. Harutyunyan, K.-H. Ernst, B. L. Feringa, *Nature* **2011**, 479, 208; b) M. Baroncini, S. Silvi, A. Credi, *Chem. Rev.* **2020**, 120, 200.
- [6] a) A. Terzopoulou, J. D. Nicholas, X.-Z. Chen, B. J. Nelson, S. Pané, J. Puigmartí-Luis, *Chem. Rev.* **2020**, 120, 11175; b) M. Fernández-Medina, M. A. Ramos-Docampo, O. Hovorka, V. Salgueiriño, B. Städler, *Adv. Funct. Mater.* **2020**, 30, 1908283; c) H. Zhou, C. C. Mayorga-Martinez, S. Pané, L. Zhang, M. Pumera, *Chem. Rev.* **2021**, 121, 4999; d) Y. Tu, F. Peng, D. A. Wilson, *Adv. Mater.* **2017**, 29, 1701970.
- [7] a) A. Credi, *Angew. Chem., Int. Ed.* **2014**, 53, 4274; b) B. Khezri, M. Pumera, *Adv. Mater.* **2019**, 31, 1806530.
- [8] a) B. L. Feringa, *Adv. Mater.* **2020**, 32, 1906416; b) F. Soto, E. Karshalev, F. Zhang, B. E. Fernandez de Avila, A. Nourhani, J. Wang, *Chem. Rev.* **2022**, 122, 5365; c) X. Zhang, Q. Fu, H. Duan, J. Song, H. Yang, *ACS Nano* **2021**, 15, 6147.
- [9] a) R. F. Dong, Y. Hu, Y. F. Wu, W. Gao, B. Y. Ren, Q. L. Wang, Y. P. Cai, *J. Am. Chem. Soc.* **2017**, 139, 1722; b) Y. Ying, M. Pumera, *Chem. - Eur. J.* **2019**, 25, 106; c) Z. Lin, C. Gao, D. Wang, Q. He, *Angew. Chem., Int. Ed.* **2021**, 60, 8750; d) P. Díez, E. Lucena-Sánchez, A. Escudero, A. Llopis-Lorente, R. Villalonga, R. Martínez-Máñez, *ACS Nano* **2021**, 15, 4467; e) X. Liu, X. Sun, Y. Peng, Y. Wang, D. Xu, W. Chen, W. Wang, X. Yan, X. Ma, *ACS Nano* **2022**, 16, 14666; f) L. Dekanovsky, Y. Ying, J. Zelenka, J. Plutnar, S. M. Beladi-Mousavi, I. Křížová, F. Novotný, T. Ruml, M. Pumera, *Adv. Funct. Mater.* **2022**, 32, 2205062; g) M. Yuan, M. Gong, H. Huang, Y. Zhao, Y. Ying, S. Wang, *Inorg. Chem. Front.* **2022**, 9, 5725.
- [10] a) C. Chen, F. Soto, E. Karshalev, J. Li, J. Wang, *Adv. Funct. Mater.* **2019**, 29, 1806290; b) B. E. Fernández de Avila, W. Gao, E. Karshalev, L. Zhang, J. Wang, *Acc. Chem. Res.* **2018**, 51, 1901; c) L. Ren, W. Wang, T. E. Mallouk, *Acc. Chem. Res.* **2018**, 51, 1948.
- [11] a) Z. Xiao, S. Duan, P. Xu, J. Cui, H. Zhang, W. Wang, *ACS Nano* **2020**, 14, 8658; b) Y. Sun, J. Jiang, G. Zhang, N. Yuan, H. Zhang, B. Song, B. Dong, *Langmuir* **2021**, 37, 180; c) M. Liu, L. Chen, Z. Zhao, M. Liu, T. Zhao, Y. Ma, Q. Zhou, Y. S. Ibrahim, A. A. Elzatahry, X. Li, D. Zhao, *J. Am. Chem. Soc.* **2022**, 144, 3892; d) M. Urso, M. Ussia, M. Pumera, *Adv. Funct. Mater.* **2021**, 31, 2101510.
- [12] a) X. Wang, X.-Z. Chen, C. C. J. Alcántara, S. Sevim, M. Hoop, A. Terzopoulou, C. de Marco, C. Hu, A. J. de Mello, P. Falcara, S. Furukawa, B. J. Nelson, J. Puigmartí-Luis, S. Pané, *Adv. Mater.* **2019**, 31, 1970192; b) J. Vyskočil, C. C. Mayorga-Martinez, E. Jablonská, F. Novotný, T. Ruml, M. Pumera, *ACS Nano* **2020**, 14, 8247.
- [13] a) T. Fu, Y. Ma, *Chem. Eng. Sci.* **2015**, 135, 343; b) M. Motegh, J. R. van Ommen, P. W. Appel, R. F. Mudde, M. T. Kreuzer, *Chem. Eng. Sci.* **2013**, 100, 506; c) A. Bhanawat, K. Zhu, L. Pilon, *Sustainable Energy Fuels* **2022**, 6, 910; d) C. Yao, Y. Liu, S. Zhao, Z. Dong, G. Chen, *AIChE J.* **2017**, 63, 1727; e) L. Guo, Y. Liu, P. Ran, G. Wang, J. Shan, X. Li, C. Liu, J. Li, *Microsyst. Nanoeng.* **2022**, 8, 34.
- [14] a) Q. Yang, L. Xu, W. Zhong, Q. Yan, Y. Gao, W. Hong, Y. She, G. Yang, *Adv. Intell. Syst.* **2020**, 2, 2000049; b) S. Mohanty, I. S. M. Khalil, S. Misra, *Proc. R. Soc. A* **2020**, 476, 20200621; c) L. Ren, N. Nama, J. M. McNeill, F. Soto, Z. Yan, W. Liu, W. Wang, J. Wang, T. E. Mallouk, *Sci. Adv.* **2019**, 5, eaax3084; d) Y. Dou, C. A. Cartier, W. Fei, S. Pandey, S. Razavi, I. Kretzschmar, K. J. M. Bishop, *Langmuir* **2016**, 32, 13167; e) J. G. Lee, A. M. Brooks, W. A. Shelton, K. J. M. Bishop, B. Bharti, *Nat. Commun.* **2019**, 10, 2575.
- [15] H. Huang, J. Li, M. G. Yuan, H. W. Yang, Y. Zhao, Y. L. Ying, S. Wang, *Angew. Chem., Int. Ed.* **2022**, 61, e202211163.
- [16] a) L. Xu, F. Mou, H. Gong, M. Luo, J. Guan, *Chem. Soc. Rev.* **2017**, 46, 6905; b) K. Villa, M. Pumera, *Chem. Soc. Rev.* **2019**, 48, 4966.
- [17] S. Palagi, D. P. Singh, P. Fischer, *Adv. Opt. Mater.* **2019**, 7, 1900370.
- [18] a) L. Dai, Z. Ge, N. Jiao, L. Liu, *Small* **2019**, 15, 1902815; b) S. Palagi, A. G. Mark, S. Y. Reigh, K. Melde, T. Qiu, H. Zeng, C. Parmeggiani, D. Martella, A. Sanchez-Castillo, N. Kaperbaum, F. Giesselmann, D. S. Wiersma, E. Lauga, P. Fischer, *Nat. Mater.* **2016**, 15, 647; c) K. Yang, L. Hu, X. Ma, S. Ye, L. Cheng, X. Shi, C. Li, Y. Li, Z. Liu, *Adv. Mater.* **2012**, 24, 1868; d) H.-R. Jiang, N. Yoshinaga, M. Sano, *Phys. Rev. Lett.* **2010**, 105, 268302; e) M. Xuan, Z. Wu, J. Shao, L. Dai, T. Si, Q. He, *J. Am. Chem. Soc.* **2016**, 138, 6492; f) X. Peng, Z. Chen, P. S. Kollipara, Y. Liu, J. Fang, L. Lin, Y. Zheng, *Light: Sci. Appl.* **2020**, 9, 141.

- [19] a) Q. Zhang, R. Dong, Y. Wu, W. Gao, Z. He, B. Ren, *ACS Appl. Mater. Interfaces* **2017**, *9*, 4674; b) D. P. Singh, U. Choudhury, P. Fischer, A. G. Mark, *Adv. Mater.* **2017**, *29*, 1701328; c) Y. Wang, C. Zhou, W. Wang, D. Xu, F. Zeng, C. Zhan, J. Gu, M. Li, W. Zhao, J. Zhang, J. Guo, H. Feng, X. Ma, *Angew. Chem., Int. Ed.* **2018**, *57*, 13110; d) X. Wang, V. Sridhar, S. Guo, N. Talebi, A. Miguel-López, K. Hahn, P. A. van Aken, S. Sánchez, *Adv. Funct. Mater.* **2018**, *28*, 1705862; e) R. Dong, Q. Zhang, W. Gao, A. Pei, B. Ren, *ACS Nano* **2016**, *10*, 839; f) Y. Li, F. Mou, C. Chen, M. You, Y. Yin, L. Xu, J. Guan, *RSC Adv.* **2016**, *6*, 10697; g) X. Yan, J. Xu, Z. Meng, J. Xie, H. Wang, *Small* **2020**, *16*, 2001548.
- [20] a) J. Wang, Z. Xiong, J. Tang, *Adv. Intell. Syst.* **2021**, *3*, 2000170; b) Y. Wang, J. Yan, N. Wen, H. Xiong, S. Cai, Q. He, Y. Hu, D. Peng, Z. Liu, Y. Liu, *Biomaterials* **2020**, *230*, 119619.
- [21] a) X. Zhou, Z. Li, L. Tan, Y. Zhang, Y. Jiao, *ACS Appl. Mater. Interfaces* **2020**, *12*, 23134; b) F. Ji, D. Jin, B. Wang, L. Zhang, *ACS Nano* **2020**, *14*, 6990; c) Y. Hu, W. Liu, Y. Sun, *ACS Appl. Mater. Interfaces* **2020**, *12*, 41495.
- [22] a) Z. Deng, F. Mou, S. Tang, L. Xu, M. Luo, J. Guan, *Appl. Mater. Today* **2018**, *13*, 45; b) Y. Sun, Y. Liu, D. Zhang, H. Zhang, J. Jiang, R. Duan, J. Xiao, J. Xing, D. Zhang, B. Dong, *ACS Appl. Mater. Interfaces* **2019**, *11*, 40533.
- [23] J. A. Cohen, R. Golestanian, *Phys. Rev. Lett.* **2014**, *112*, 068302.
- [24] a) M. Xuan, J. Shao, X. Lin, L. Dai, Q. He, *Colloids Surf., A* **2015**, *482*, 92; b) Z. Wu, T. Si, W. Gao, X. Lin, J. Wang, Q. He, *Small* **2016**, *12*, 577.
- [25] A.-I. Bunea, D. Martella, S. Nocentini, C. Parmeggiani, R. Taboryski, D. S. Wiersma, *Adv. Intell. Syst.* **2021**, *3*, 2000256.
- [26] D. Bernoulli, J. Bernoulli, *Hydrodynamics and Hydraulics*, Dover Publications, New York **1968**.
- [27] Y. Zhao, M. Yuan, H. Yang, J. Li, Y. Ying, J. Li, W. Wang, S. Wang, *Small* **2023**, <https://doi.org/10.1002/sml.202305189>.
- [28] a) A. M. Pourrahimi, K. Villa, C. L. M. Palenzuela, Y. Ying, Z. Sofer, M. Pumera, *Adv. Funct. Mater.* **2019**, *29*, 1808678; b) T. Maric, M. Z. M. Nasir, R. D. Webster, M. Pumera, *Adv. Funct. Mater.* **2020**, *30*, 1908614; c) X. Peng, M. Urso, M. Pumera, *Small Methods* **2021**, *5*, 2100617.
- [29] a) J. Zhu, H. Wang, Z. Zhang, *Langmuir* **2021**, *37*, 4964; b) X. He, H. Jiang, J. Li, Y. Ma, B. Fu, C. Hu, *Small* **2021**, *17*, 2101388; c) C. M. Oral, M. Ussia, D. K. Yavuz, M. Pumera, *Small* **2022**, *18*, 2106271; d) J. Kim, S. Jo, W.-j. Lee, J. Lim, T. S. Lee, *Mater. Des.* **2022**, *219*, 110743.
- [30] Z. Ye, Y. Sun, H. Zhang, B. Song, B. Dong, *Nanoscale* **2017**, *9*, 18516.
- [31] Y. Zheng, Y. Jiao, J. Chen, J. Liu, J. Liang, A. Du, W. Zhang, Z. Zhu, S. C. Smith, M. Jaroniec, G. Q. Lu, S. Z. Qiao, *J. Am. Chem. Soc.* **2011**, *133*, 20116.
- [32] a) A. I. Campbell, S. J. Ebbens, *Langmuir* **2013**, *29*, 14066; b) K. Wolff, A. M. Hahn, H. Stark, *Eur. Phys. J. E: Soft Matter Biol. Phys.* **2013**, *36*, 43; c) C. Lozano, B. ten Hagen, H. Löwen, C. Bechinger, *Nat. Commun.* **2016**, *7*, 12828; d) B. Dai, J. Wang, Z. Xiong, X. Zhan, W. Dai, C.-C. Li, S.-P. Feng, J. Tang, *Nat. Nanotechnol.* **2016**, *11*, 1087.
- [33] D. P. Singh, W. E. Uspal, M. N. Popescu, L. G. Wilson, P. Fischer, *Adv. Funct. Mater.* **2018**, *28*, 1706660.
- [34] C. Chen, F. Mou, L. Xu, S. Wang, J. Guan, Z. Feng, Q. Wang, L. Kong, W. Li, J. Wang, Q. Zhang, *Adv. Mater.* **2017**, *29*, 1603374.
- [35] Y. Ying, J. Plutnar, M. Pumera, *Small* **2021**, *17*, 2100294.
- [36] M. Urso, M. Ussia, F. Novotný, M. Pumera, *Nat. Commun.* **2022**, *13*, 3573.
- [37] X. Lyu, X. Liu, C. Zhou, S. Duan, P. Xu, J. Dai, X. Chen, Y. Peng, D. Cui, J. Tang, X. Ma, W. Wang, *J. Am. Chem. Soc.* **2021**, *143*, 12154.
- [38] S. K. Srivastava, G. Clergeaud, T. L. Andresen, A. Boisen, *Adv. Drug Delivery Rev.* **2018**, *138*, 41.
- [39] Y. Duan, B. Liu, *Adv. Mater.* **2018**, *30*, 1802394.
- [40] a) I. De Vlaminck, C. Dekker, *Annu. Rev. Biophys.* **2012**, *41*, 453; b) W. Wang, L. A. Castro, M. Hoyos, T. E. Mallouk, *ACS Nano* **2012**, *6*, 6122; c) B. E. Fernández de Ávila, C. Angell, F. Soto, M. A. Lopez-Ramirez, D. F. Báez, S. Xie, J. Wang, Y. Chen, *ACS Nano* **2016**, *10*, 4997; d) D. Ahmed, T. Baasch, B. Jang, S. Pane, J. Dual, B. J. Nelson, *Nano Lett.* **2016**, *16*, 4968; e) A. Ozcelik, J. Rufo, F. Guo, Y. Gu, P. Li, J. Lata, T. J. Huang, *Nat. Methods* **2018**, *15*, 1021.
- [41] a) L. S. Zheng, Y. J. Jia, D. R. Dong, W. Lam, D. F. Li, H. B. Ji, D. Sun, *IEEE Trans. Rob.* **2022**, *38*, 1583; b) D. D. Jin, L. Zhang, *Acc. Chem. Res.* **2022**, *55*, 98; c) Q. Q. Wang, L. Zhang, *ACS Nano* **2021**, *15*, 149.
- [42] X. Chen, M. Hoop, F. Mushtaq, E. Siringil, C. Hu, B. J. Nelson, S. Pané, *Appl. Mater. Today* **2017**, *9*, 37.
- [43] a) Y. Dong, L. Wang, V. Iacovacci, X. Wang, L. Zhang, B. J. Nelson, *Matter* **2022**, *5*, 77; b) K. E. Peyer, L. Zhang, B. J. Nelson, *Nanoscale* **2013**, *5*, 1259.
- [44] a) X. Li, T. Fukuda, *Micromachines* **2020**, *11*, 697; b) W. Gao, A. Uygun, J. Wang, *J. Am. Chem. Soc.* **2012**, *134*, 897.
- [45] B. Qiu, L. Xie, J. Zeng, T. Liu, M. Yan, S. Zhou, Q. Liang, J. Tang, K. Liang, B. Kong, *Adv. Funct. Mater.* **2021**, *31*, 2010694.
- [46] H. Yu, J. Yang, *Microfluid Nanofluidics* **2021**, *25*, 72.
- [47] L. Zhang, T. Petit, Y. Lu, B. E. Kratochvil, K. E. Peyer, R. Pei, J. Lou, B. J. Nelson, *ACS Nano* **2010**, *4*, 6228.
- [48] Y. Alapan, U. Bozuyuk, P. Erkoc, A. C. Karacakol, M. Sitti, *Sci. Robo.* **2020**, *5*, eaba5726.
- [49] S. Yu, T. Li, F. Ji, S. Zhao, K. Liu, Z. Zhang, W. Zhang, Y. Mei, *Mater. Today Adv.* **2022**, *14*, 100231.
- [50] Q. Brosseau, F. B. Usabiaga, E. Lushi, Y. Wu, L. Ristroph, M. D. Ward, M. J. Shelley, J. Zhang, *Soft Matter* **2021**, *17*, 6597.
- [51] D. J. Bell, S. Leutenegger, K. M. Hammar, L. X. Dong, B. J. Nelson, in *Proc. 2007 IEEE Int. Conf. Robotics Automation*, IEEE, Piscataway, NJ **2007**, pp. 1128–1133.
- [52] a) L. Zhang, J. J. Abbott, L. X. Dong, B. E. Kratochvil, D. Bell, B. J. Nelson, *Appl. Phys. Lett.* **2009**, *94*, 064107; b) A. Servant, F. M. Qiu, M. Mazza, K. Kostarelos, B. J. Nelson, *Adv. Mater.* **2015**, *27*, 2981.
- [53] a) K. E. Peyer, S. Tottori, F. Qiu, L. Zhang, B. J. Nelson, *Chem. - Eur. J.* **2013**, *19*, 28; b) Z. Wang, D. Fu, D. Xie, S. Fu, J. Wu, S. Wang, F. Wang, Y. Ye, Y. Tu, F. Peng, *Adv. Funct. Mater.* **2021**, *31*, 2101648; c) A. W. Mahoney, J. C. Sarrazin, E. Bamberg, J. J. Abbott, *Adv. Rob.* **2011**, *25*, 1007.
- [54] a) Z. G. Wu, J. Troll, H. H. Jeong, Q. Wei, M. Stang, F. Ziemssen, Z. G. Wang, M. D. Dong, S. Schnichels, T. Qiu, P. Fischer, *Sci. Adv.* **2018**, *4*, eaat4388; b) P. J. Vach, D. Walker, P. Fischer, P. Fratzl, D. Faivre, *J. Phys. D* **2017**, *50*, 11LT03; c) X. H. Yan, Q. Zhou, M. Vincent, Y. Deng, J. F. Yu, J. B. Xu, T. T. Xu, T. Tang, L. M. Bian, Y. X. J. Wang, K. Kostarelos, L. Zhang, *Sci. Rob.* **2017**, *2*, eaq1155; d) J. Li, S. Sattayasamitsathit, R. Dong, W. Gao, R. Tam, X. Feng, S. Ai, J. Wang, *Nanoscale* **2014**, *6*, 9415; e) W. Zhuge, X. Ding, W. Zhang, D. Zhang, H. Wang, J. Wang, *Chem. Eng. J.* **2022**, *447*, 137455; f) D. Gong, J. Cai, N. Celi, L. Feng, Y. Jiang, D. Zhang, *J. Magn. Magn. Mater.* **2018**, *468*, 148.
- [55] V. de la Asunción-Nadal, C. Franco, A. Veciana, S. Ning, A. Terzopoulou, S. Sevím, X.-Z. Chen, D. Gong, J. Cai, P. D. Wendel-García, B. Jurado-Sánchez, A. Escarpa, J. Puigmartí-Luis, S. Pané, *Small* **2022**, *18*, 2203821.
- [56] a) S. Tottori, L. Zhang, F. M. Qiu, K. Krawczyk, A. Franco-Obregon, B. J. Nelson, *Adv. Mater.* **2012**, *24*, 811; b) X. P. Wang, X. H. Qin, C. Z. Hu, A. Terzopoulou, X. Z. Chen, T. Y. Huang, K. Maniura-Weber, S. Pane, B. J. Nelson, *Adv. Funct. Mater.* **2018**, *28*, 1804107.
- [57] H. Yu, W. Tang, G. Mu, H. Wang, X. Chang, H. Dong, L. Qi, G. Zhang, T. Li, *Micromachines* **2018**, *9*, 540.
- [58] J. Law, H. Chen, Y. Wang, J. Yu, Y. Sun, *Sci. Adv.* **2022**, *8*, eade3161.
- [59] a) H.-W. Huang, M. S. Sakar, A. J. Petruska, S. Pané, B. J. Nelson, *Nat. Commun.* **2016**, *7*, 12263; b) M. Hoop, A. S. Ribeiro, D. Rösch, P. Weinand, N. Mendes, F. Mushtaq, X.-Z. Chen, Y. Shen, C. F. Pujante, J. Puigmartí-Luis, J. Paredes, B. J. Nelson, A. P. Pêgo, S. Pané, *Adv. Funct. Mater.* **2018**, *28*, 1705920.
- [60] A. Farzin, S. A. Etesami, J. Quint, A. Memic, A. Tamayol, *Adv. Healthcare Mater.* **2020**, *9*, 1901058.

- [61] N. Murali, S. K. Rainu, N. Singh, S. Betal, *Biosens. Bioelectron.: X* **2022**, 11, 100206.
- [62] C. Pauer, A. Venczel, M. Dass, T. Liedl, J. Tavacoli, *Adv. Mater.* **2022**, 7, 2200450.
- [63] a) L. Schwarz, D. D. Karnaushenko, F. Hebenstreit, R. Naumann, O. G. Schmidt, M. Medina-Sánchez, *Adv. Sci.* **2020**, 7, 2000843; b) L. Liu, J. Wu, S. Wang, L. Kun, J. Gao, B. Chen, Y. Ye, F. Wang, F. Tong, J. Jiang, J. Ou, D. A. Wilson, Y. Tu, F. Peng, *Nano Lett.* **2021**, 21, 3518; c) Z. Lin, X. Fan, M. Sun, C. Gao, Q. He, H. Xie, *ACS Nano* **2018**, 12, 2539; d) D. Fu, J. Jiang, S. Fu, D. Xie, C. Gao, Y. Feng, S. Liu, Y. Ye, L. Liu, Y. Tu, F. Peng, *Adv. Healthcare Mater.* **2023**, 12, 2300737.
- [64] J. An, H. Hong, M. Won, H. Rha, Q. Ding, N. Kang, H. Kang, J. S. Kim, *Chem. Soc. Rev.* **2023**, 52, 30.
- [65] B. Wang, K. F. Chan, K. Yuan, Q. Q. Wang, X. F. Xia, L. D. Yang, H. Ko, Y. X. J. Wang, J. J. Y. Sung, P. W. Y. Chiu, L. Zhang, *Sci. Rob.* **2021**, 6, eabd2813.
- [66] Q. Q. Wang, X. Z. Du, D. D. Jin, L. Zhang, *ACS Nano* **2022**, 16, 604.
- [67] Y. B. Zhang, L. Zhang, L. D. Yang, C. I. Vong, K. F. Chan, W. K. K. Wu, T. N. Y. Kwong, N. W. S. Lo, M. Ip, S. H. Wong, J. J. Y. Sung, P. W. Y. Chiu, L. Zhang, *Sci. Adv.* **2019**, 5, eaau9650.
- [68] M. M. Sun, K. F. Chan, Z. F. Zhang, L. Wang, Q. L. Wang, S. H. Yang, S. M. Chan, P. W. Y. Chiu, J. J. Y. Sung, L. Zhang, *Adv. Mater.* **2022**, 34, 2201888.
- [69] a) K. J. Rao, F. Li, L. Meng, H. Zheng, F. Cai, W. Wang, *Small* **2015**, 11, 2836; b) C. Zhou, L. Zhao, M. Wei, W. Wang, *ACS Nano* **2017**, 11, 12668; c) X. Lu, Y. Wei, H. Ou, C. Zhao, L. Shi, W. Liu, *Small* **2021**, 17, 2104516; d) T. Xu, F. Soto, W. Gao, R. Dong, V. Garcia-Gradilla, E. Magaña, X. Zhang, J. Wang, *J. Am. Chem. Soc.* **2015**, 137, 2163.
- [70] A. Mojahed, M. Rajabi, *Ultrasonics* **2018**, 86, 1.
- [71] a) G. Loget, A. Kuhn, *Nat. Commun.* **2011**, 2, 535; b) Y. Yoshizumi, T. Honegger, K. Berton, H. Suzuki, D. Peyrade, *Small* **2015**, 11, 5630; c) A. M. Brooks, S. Sabrina, K. J. M. Bishop, *Proc. Natl. Acad. Sci. USA* **2018**, 115, E1090; d) Z. Wang, W. Xu, Z. Wang, D. Lyu, Y. Mu, W. Duan, Y. Wang, *J. Am. Chem. Soc.* **2021**, 143, 19881.
- [72] a) J. Roche, S. Carrara, J. Sanchez, J. Lannelongue, G. Loget, L. Bouffier, P. Fischer, A. Kuhn, *Sci. Rep.* **2014**, 4, 6705; b) S. T. Chang, V. N. Paunov, D. N. Petsev, O. D. Velev, *Nat. Mater.* **2007**, 6, 235.
- [73] a) A. M. Drews, H.-Y. Lee, K. J. M. Bishop, *Lab Chip* **2013**, 13, 4295; b) C. A. Cartier, A. M. Drews, K. J. M. Bishop, *Lab Chip* **2014**, 14, 4230; c) A. M. Drews, C. A. Cartier, K. J. M. Bishop, *Langmuir* **2015**, 31, 3808.
- [74] a) E. Yariv, *Phys. Fluids* **2005**, 17, 051702; b) M. Z. Bazant, T. M. Squires, *Phys. Rev. Lett.* **2004**, 92, 066101; c) D. Saintillan, E. Darve, E. S. G. Shaqfeh, *J. Fluid Mech.* **2006**, 563, 223; d) M. S. Kilic, M. Z. Bazant, *Electrophoresis* **2011**, 32, 614.
- [75] R. Zhuang, D. Zhou, X. Chang, Y. Mo, G. Zhang, L. Li, *Appl. Mater. Today* **2022**, 26, 101314.
- [76] H. Joh, D. Fan, in *Field-Driven Micro and Nanorobots for Biology and Medicine* (Eds: Y. Sun, X. Wang, J. Yu), Springer International Publishing, Cham **2022**, pp. 113–131.
- [77] a) Y. F. Gao, M. J. Cheng, B. L. Wang, Z. G. Feng, F. Shi, *Adv. Mater.* **2010**, 22, 5125; b) G. Ju, M. Cheng, M. Xiao, J. Xu, K. Pan, X. Wang, Y. Zhang, F. Shi, *Adv. Mater.* **2013**, 25, 2915; c) M. M. Song, M. J. Cheng, G. N. Ju, Y. J. Zhang, F. Shi, *Adv. Mater.* **2014**, 26, 7059.
- [78] Y. Chu, L. Qin, L. Zhen, Q. Pan, *ACS Appl. Mater. Interfaces* **2018**, 10, 24899.
- [79] Y. Wang, L. W. Zhang, Y. R. Guo, Y. Gan, G. Liu, D. Y. Zhang, H. W. Chen, *Small* **2021**, 17, 2103423.
- [80] H. Chen, Q. Zhao, Y. Wang, S. Mu, H. Cui, J. Wang, T. Kong, X. Du, *ACS Appl. Mater. Interfaces* **2019**, 11, 15927.
- [81] T. Luan, F. Meng, P. Tao, W. Shang, J. Wu, C. Song, T. Deng, *Small* **2019**, 15, e1804959.
- [82] Y. C. Tang, M. T. Li, T. L. Wang, X. G. Dong, W. Q. Hu, M. T. Sitti, *Adv. Mater.* **2022**, 34, 2204185.
- [83] D. Pan, D. Wu, P. J. Li, S. Y. Ji, X. Nie, S. Y. Fan, G. Y. Chen, C. C. Zhang, C. Xin, B. Xu, S. W. Zhu, Z. Cai, Y. L. Hu, J. W. Li, J. R. Chu, *Adv. Funct. Mater.* **2021**, 31, 2009386.
- [84] P. Feng, X. Du, J. Guo, K. Wang, B. Song, *ACS Appl. Mater. Interfaces* **2021**, 13, 8985.
- [85] Y. Zhang, H. Zhu, W. X. Qiu, Y. L. Zhou, G. S. Huang, Y. F. Mei, A. A. Solovev, *Chem. Commun.* **2018**, 54, 5692.
- [86] Z. Guo, T. Wang, A. Rawal, J. Hou, Z. Cao, H. Zhang, J. Xu, Z. Gu, V. Chen, K. Liang, *Mater. Today* **2019**, 28, 10.
- [87] Z. Guo, Y. Wu, Z. Xie, J. Shao, J. Liu, Y. Yao, J. Wang, Y. Shen, J. J. Gooding, K. Liang, *Angew. Chem., Int. Ed.* **2022**, 61, e202209747.
- [88] H. Huang, Y. Zhao, H. Yang, J. Li, Y. Ying, J. Li, S. Wang, *Nanoscale* **2023**, 15, 14165.
- [89] F. Novotny, M. Pumera, *Sci. Rep.* **2019**, 9, 13222.
- [90] a) F. Novotný, J. Plutnar, M. Pumera, *Adv. Funct. Mater.* **2019**, 29, 1903041; b) Z. F. Wang, Y. Yan, C. Li, Y. Yu, S. Cheng, S. Chen, X. J. Zhu, L. P. Sun, W. Tao, J. W. Liu, F. Wang, *ACS Nano* **2022**, 16, 9019; c) Y. F. Zhang, H. Hess, *Nat. Rev. Chem.* **2021**, 5, 500.
- [91] E. Jensen, D. Crossman, *Anat. Rec.* **2014**, 297, 2227.
- [92] a) A. Martinez-Marrades, J. F. Rupprecht, M. Gross, G. Tessier, *Opt. Express* **2014**, 22, 29191; b) V. Brasiliense, A. N. Patel, A. Martinez-Marrades, J. Shi, Y. Chen, C. Combellas, G. Tessier, F. Kanoufi, *J. Am. Chem. Soc.* **2016**, 138, 3478; c) M.-C. Nguyen, P. Berto, F. Valentino, J.-F. Lemineur, J.-M. Noel, F. Kanoufi, G. Tessier, *ACS Nano* **2022**, 16, 14422.
- [93] a) A. Aziz, M. Medina-Sanchez, N. Koukourakis, J. W. Wang, R. Kuschmierz, H. Radner, J. W. Czarske, O. G. Schmidt, *Adv. Funct. Mater.* **2019**, 29, 1905272; b) A. Aziz, J. Holthof, S. Meyer, O. G. Schmidt, M. Medina-Sanchez, *Adv. Healthcare Mater.* **2021**, 10, 2101077.
- [94] J.-M. B. A. Sulzmann, J. Jacot, presented at Proc. Int. Solid State Sensors Actuators Conf. (Transducers '97), Chicago, IL, USA, June **1997**.
- [95] D. von Wangenheim, R. Hauschild, M. Fendrych, V. Barone, J. Friml, *Elife* **2017**, 6, 116285.
- [96] A. McGlasson, L. C. Bradley, *Small* **2021**, 17, 2104926.
- [97] H. Ye, Y. Wang, X. J. Liu, D. D. Xu, H. Yuan, H. Q. Sun, S. B. Wang, X. Ma, *J. Colloid Interface Sci.* **2021**, 588, 510.



Hai Huang received his Master's degree in the School of Materials Science and Engineering from the Zhejiang Sci-Tech University in 2023. He is currently a Ph.D. student in the School of Materials and Energy at the University of Electronic Science and Technology of China. His research interests focus on MOFs' synthesis and their application in micro-/nanomotors and sodium-ion batteries.



Shihao Yang received his BE and M.E. from the School of Materials Science and Engineering at the Harbin Institute of Technology in 2018 and 2020, respectively. He is currently working toward his Ph.D. in the Department of Mechanical and Automation Engineering at The Chinese University of Hong Kong. His research interests include micro-/nanorobots and their collective behaviors.



Yulong Ying is an Associate Professor in the School of Materials Science and Engineering at Zhejiang Sci-Tech University. He received his Ph.D. degree from the School of Materials Science and Engineering, Zhejiang University (China, 2017). He has been a Senior Scientist in the Center for Advanced Functional Nanorobots at the University of Chemistry and Technology, Prague (Czech Republic). His research focuses on micro-/nanomotor design with MOFs and stimuli-responsive materials for environmental remediation, green MOF synthesis, and 2D/nanostructured materials for water treatment and energy storage.



Xiangzhong Chen earned his Ph.D. in Polymer Chemistry and Physics from Nanjing University. He conducted research at the Pennsylvania State University during his studies. Afterward, he worked as a Postdoc at the ETH Zurich and later was promoted to the position of Senior Scientist. Since March 1, 2023, he is an Associate Professor at Fudan University, specializing in Ferrous Materials for Smart Biodevices. His research focuses on integrating functional ferromagnetic and ferroelectric materials into cutting-edge biomedical applications, including targeted drug delivery, tissue engineering, and neural stimulation.



Josep Puigmartí-Luis, a Chemist, earned his Master's in Chemistry and Food Engineering from the Institut Químic de Sarrià in 2003. He obtained a second Master and his Ph.D. in Materials Science at the Institut de Ciència de Materials de Barcelona. In 2019, he became an ICREA Research Professor and established his group at the UB in 2020. His research focuses on synthesizing and designing functional materials in solution and on surfaces. He also specializes in microfluidic technologies to control and study the formation and function of unique functional materials and assemblies.



Li Zhang is a Professor in the Department of Mechanical and Automation Engineering and a Professor by courtesy in the Department of Surgery at The Chinese University of Hong Kong (CUHK). He is also a Director of the Shenzhen Institutes of Advanced Technology (SIAT)–CUHK Joint Laboratory of Robotics and Intelligent Systems. Before he joined CUHK as an Assistant Professor in 2012, he worked in Prof. Bradley Nelson's group as a Postdoc and then as a Senior Scientist and Lecturer in the Institute of Robotics and Intelligent Systems, ETH Zurich, Switzerland. His main research interests include small-scale robotics and their applications for translational biomedicine.



Salvador Pané is a Professor of Materials for Robotics and Codirector of the Multi-Scale Robotics Lab (MSRL) at the ETH Zürich. He received his Ph.D. in Chemistry from the University of Barcelona in 2008 and subsequently joined MSRL as a Postdoctoral Researcher in August 2008. He has been awarded the highly competitive ERC-Starting Grant (StG) and ERCConsolidator Grant (CoG) in 2012 and 2017, respectively. Since 2023, he is elected member of the Institut d'Estudis Catalans in the section of Science and Technology. His interests lie in bridging materials science, chemistry, and electrochemistry with small-scale robotics for various applications.